Environment International 166 (2022) 107366

Contents lists available at ScienceDirect

Environment International

journal homepage: www.elsevier.com/locate/envint

Full length article

# Exposure to naphthalene and β-pinene-derived secondary organic aerosol induced divergent changes in transcript levels of BEAS-2B cells

Michal Pardo [a,*], Svenja Offer [b,c], Elena Hartner [b,c], Sebastiano Di Bucchianico [b], Christoph Bisig [b], Stefanie Bauer [b], Jana Pantzke [b,c], Elias J. Zimmermann [b,c], Xin Cao [b,c], Stephanie Binder [b,c], Evelyn Kuhn [b], Anja Huber [b], Seongho Jeong [b,c], Uwe Käfer [b,c], Eric Schneider [c], Arunas Mesceriakovas [d], Jan Bendl [b,e,f], Ramona Brejcha [b], Angela Buchholz [g], Daniela Gat [a], Thorsten Hohaus [h], Narges Rastak [b], Erwin Karg [b], Gert Jakobi [b], Markus Kalberer [i], Tamara Kanashova [j], Yue Hu [k], Christoph Ogris [k], Annalisa Marsico [k], Fabian Theis [k], Tali Shalit [l], Thomas Gröger [b], Christopher P. Rüger [c], Sebastian Oeder [b], Jürgen Orasche [b], Andreas Paul [h], Till Ziehm [h], Zhi-Hui Zhang [i], Thomas Adam [b,e], Olli Sippula [d], Martin Sklorz [b], Jürgen Schnelle-Kreis [b], Hendryk Czech [b,c], Astrid Kiendler-Scharr [h], Ralf Zimmermann [b,c], Yinon Rudich [a]

[a] Department of Earth and Planetary Sciences, Faculty of Chemistry, Weizmann Institute of Science, 234 Herzl Street, POB 26, ISR-7610001 Rehovot, Israel
[b] Joint Mass Spectrometry Center (JMSC) at Comprehensive Molecular Analytics (CMA), Helmholtz Zentrum München, Ingolstädter Landstr. 1, D-85764 Neuherberg, Germany
[c] Joint Mass Spectrometry Center (JMSC) at Analytical Chemistry, Institute of Chemistry, University of Rostock, Dr.-Lorenz-Weg 2, D-18059 Rostock, Germany
[d] Department of Environmental and Biological Sciences, University of Eastern Finland, Yliopistonranta 1, P.O. Box 1627, FI-70210 Kuopio, Finland
[e] University of the Bundeswehr Munich, Institute for Chemistry and Environmental Engineering, Werner- Heisenberg-Weg 39, D-85577 Neubiberg, Germany
[f] Institute for Environmental Studies, Faculty of Science, Charles University, Albertov 6, CZE-12800 Prague, Czech Republic
[g] Department of Applied Physics, University of Eastern Finland, Yliopistonranta 1, P.O. Box 1627, FI-70210 Kuopio, Finland
[h] Institute of Energy and Climate Research, Troposphere (IEK-8), Forschungszentrum Jülich GmbH, Wilhelm-Johen-Str., D-52428 Jülich, Germany
[i] Department of Environmental Sciences, University of Basel, Klingelbergstr. 27, CH-4056 Basel, Switzerland
[j] Max-Delbrück-Centrum für Molekulare Medizin (MDC), Robert-Rössle-Str. 10, D-13125 Berlin, Germany
[k] Institute of Computational Biology, Helmholtz Zentrum München, Ingolstädter Landstr. 1, D-85764 Neuherberg, Germany
[l] The Mantoux Bioinformatics Institute of the Nancy and Stephen Grand Israel National Center for Personalized Medicine, Weizmann Institute of Science, Rehovot 76100, Israel

ARTICLE INFO

Handling Editor: Adrian Covaci

*Keywords:*
RNA sequencing
Soot particles
Health effects
Cytotoxicity

ABSTRACT

The health effects of exposure to secondary organic aerosols (SOAs) are still limited. Here, we investigated and compared the toxicities of soot particles (SP) coated with β-pinene SOA ($SOA_{βPin}$-SP) and SP coated with naphthalene SOA ($SOA_{Nap}$-SP) in a human bronchial epithelial cell line (BEAS-2B) residing at the air–liquid interface. $SOA_{βPin}$-SP mostly contained oxygenated aliphatic compounds from β-pinene photooxidation, whereas $SOA_{Nap}$-SP contained a significant fraction of oxygenated aromatic products under similar conditions. Following exposure, genome-wide transcriptome responses showed an Nrf2 oxidative stress response, particularly for $SOA_{Nap}$-SP. Other signaling pathways, such as redox signaling, inflammatory signaling, and the involvement of

*Abbreviations:* AMS, aerosol mass spectrometry; ALI, air-liquid interphase; ALDH, aldehyde dehydrogenase; CA, clean air; CAST, Combustion Aerosol Standard; Cyp, Cytochrome P450; DEG, differentially expressed genes; DEP, diesel engine exhaust; DIP-MS, direct inlet probe mass spectrometry; EC, elemental carbon; ESI, electrospray ionization; GCLM, Glutamate-cysteine ligase regulatory subunit; HMOX-1, hemeoxygenase-1; HSD, honestly significant difference; AhR, hydrocarbon receptor; IPA, Ingenuity Pathway Analysis; MDA, malondialdehyde; MMP, matrix metalloproteinase; MAPK, mitogen-activated protein kinases; NQO-1, NAD(P)H dehydrogenase quinone-1; OPROSI, Online Particle-bound Reactive Oxygen Species Instrument; OC, organic carbon; OFR, oxidation flow reactor; PM, particulate matter; RNS, reactive nitrogen species; ROS, reactive oxygen species; RNA-seq, RNA sequencing; SOAs, secondary organic aerosols; STAT3, signal transducer and activator of transcription-3; SP, soot particles; SOA-SP, SP coated by SOA; UHR-MS, ultrahigh resolution mass spectrometry; VOCs, volatile organic compounds; WHO, World Health Organization.

* Corresponding author.
*E-mail address:* michal.levin@weizmann.ac.il (M. Pardo).

https://doi.org/10.1016/j.envint.2022.107366
Received 7 March 2022; Received in revised form 13 May 2022; Accepted 17 June 2022
Available online 21 June 2022

Signaling pathway
Particulate matter

matrix metalloproteinase, were identified to have a stronger impact following exposure to $SOA_{Nap}$-SP. $SOA_{Nap}$-SP also induced a stronger genotoxicity response than that of $SOA_{\beta Pin}$-SP. This study elucidated the mechanisms that govern SOA toxicity and showed that, compared to SOAs derived from a typical biogenic precursor, SOAs from a typical anthropogenic precursor have higher toxicological potency, which was accompanied with the activation of varied cellular mechanisms, such as aryl hydrocarbon receptor. This can be attributed to the difference in chemical composition; specifically, the aromatic compounds in the naphthalene-derived SOA had higher cytotoxic potential than that of the β-pinene-derived SOA.

## 1. Introduction

Massive urbanization and industrialization have increased particulate matter (PM) levels in the atmosphere, generating high loading of mixed organics/inorganics particles, including soot particles (SP), dust, and smoke from biomass burning (Brauer et al., 2016; Manisalidis et al., 2020; Pöschl and Shiraiwa, 2015; Schnitzler et al., 2014). A dominant component of atmospheric PM is secondary organic aerosols (SOAs), which are formed through the oxidation of volatile organic compounds (VOCs) from biogenic and anthropogenic sources (Nault et al., 2021). More biogenic VOCs are emitted to the atmosphere globally than regionally (Borbon et al., 2013; Gu et al., 2021; Guenther et al., 1995). However, on regional scales and in urban locations, anthropogenic VOCs may dominate (Borbon et al., 2013; Gu et al., 2021). Atmospheric SOA formation is complex and includes gas-phase photochemical reactions with ozone, OH, $NO_3$, $NO_x$, and reactive hydrocarbons (Kolb and Worsnop, 2012; Kroll and Seinfeld 2008; Lim et al., 2019). SOA composition is convoluted and consists of a large variety of complex organic compounds (Nault et al., 2021). These secondary compounds either nucleate and form new particles or condense onto existing particles such as soot or dust, creating complex organic matrix coating (Schnitzler et al., 2014). Therefore, understanding the relationship between the toxicity of SOA-coated particles, their chemical composition, and how atmospheric aging modifies the toxicity is a key to determine their effects on the climate and human health.

Exposure to ambient PM has been associated with significant adverse health outcomes that in part account for high morbidity, and mortality worldwide (Burnett et al., 2018; Cohen et al., 2017; Forouzanfar et al., 2016; Manisalidis et al., 2020; Nault et al., 2021). As a result, the World Health Organization (WHO) has recently updated its guidelines, reducing PM recommendations even more (World Health 2021). Toxicology studies suggest that the possible mechanisms for PM-induced health effects are through PM-induced oxidants production (such as reactive oxygen and nitrogen species ROS/RNS) and oxidative stress, inflammatory response, cellular damage, and death (Al Housseiny et al., 2020; Bai et al., 2017; Burnett et al., 2018; De Grove et al., 2018; Longhin et al., 2018; Wang et al., 2017; Zheng et al., 2017). To date, several studies have examined the toxicity induced by exposure to SOA (Khan et al., 2021; Lund et al., 2013; Tuet et al., 2017a; Tuet et al., 2017b). We have previously shown that exposure to SP coated with naphthalene SOA leads to a stronger toxic response compared to that of SP coated with β-pinene SOA in A549 cells and in a coculture model containing A549 cells and EA.hy926 hybrid human endothelial cells (Offer et al., 2022). It was also shown that aged SOAs from α-pinene and naphthalene in the absence of NOx contained more ROS than fresh SOA and induced a strong cell death response in A549 cells (Chowdhury et al., 2019). Furthermore, at a high dose of 10 μg/mL, extracts from α-pinene, *m*-xylene, and trimethylbenzene SOA increased the expression of the hemeoxygenase-1 (*HMOX-1)* gene in both bronchial epithelial BEAS-2B cells and macrophage-like U937 cells (Ito et al., 2019). Taken together, these studies highlight the role of chemical composition in determining the toxicities of SOA. While there have been several recent studies regarding the health effects of SOA (Chowdhury et al., 2019; Chowdhury et al., 2018; Han et al., 2020; Ito et al., 2019; Khan et al., 2021; Tuet et al., 2017a), there are still important knowledge gaps in comparison with those of primary aerosols, but also in comparison between anthropogenic and biogenic toxicities, that have not yet been addressed.

Recent technological advances enable the use of RNA sequencing (RNA-seq) to uncover multiple facets at the transcript level. RNA-seq allows the relative changes in each transcript to be quantified under specific treatment conditions or during defined developmental stages (Han et al., 2015; Koch et al., 2018). RNA-seq is not limited to selected probes on an array and can be applied to the whole genome for expression patterns that have not yet been established (Han et al., 2015). Therefore, RNA-seq may be an appropriate tool to understand biological complexity and facilitate biologically relevant changes in SOA toxicity.

This study investigates genome-wide activation pathways of exposure to low levels of SP with a low content of organic matter and SP coated by SOA (SOA-SP) on BEAS-2B lung cells (non-tumorigenic lung cells). For this purpose, two chemically different SOA precursors that represent biogenic or anthropogenic sources with different chemical characteristics were chosen. Important biogenic compounds involved in aerosol formation are monoterpenes (Alves and Pio, 2005; Mehra et al., 2020; Ylisirniö et al., 2020) such as β-pinene ($C_{10}H_{16}$), which is released by vegetation (Kopaczyk et al., 2020). Naphthalene is among the most abundant anthropogenic VOCs ($C_{10}H_8$, a polycyclic aromatic hydrocarbon, PAH) and is emitted from coal and wood combustion, traffic exhaust and petroleum distillation (Han et al., 2020; Jia and Batterman, 2010). Thus, in this study, SP coated with SOA from either naphthalene or β-pinene, were photochemically generated (predominantly by OH oxidation) in an oxidation flow reactor (OFR), and were then exposed to BEAS-2B cells grown at the air–liquid interphase (ALI). Cellular responses induced by SOA-SP exposure, including cell viability, DNA damage, and cytokine secretion, were measured. Gene expression profiling was carried out using RNA-seq followed by pathway enrichment analyses to identify biological pathways to provide a mechanistic understanding of SOA-SP-induced health effects.

## 2. Methods

### 2.1. Generation of SP, $SOA_{\beta Pin}$-SP, or $SOA_{Nap}$-SP

SOAs of naphthalene (Sigma-Aldrich, 99%, GE) or β-pinene (Sigma-Aldrich, ≥ 99%, GE) were produced by OH-dominated photooxidation in a potential aerosol mass (PAM) (Kang et al., 2007; Lambe et al., 2011) oxidation flow reactor (OFR), consisting of a metal cylinder and operated in OFR185 mode (Bruns et al., 2015; Lambe et al., 2011). The SOA condensed onto SP, which are low in organic carbon, from a Combustion Aerosol STandard (CAST) soot generator (Jing Inc) with propane fuel. Fresh SP were used as a reference control. Detailed information regarding the aerosol generation is described in Offer et al. (2022).

### 2.2. Physical and chemical characterization of SP, $SOA_{\beta Pin}$-SP or $SOA_{Nap}$-SP

Particle number and particle size distributions were evaluated using a scanning mobility particle sizer (SMPS) (Condensation particle counter (CPC), TSI Model 3775low, and a DMA (differential mobility analyzer, TSI Model 3082, USA). Equivalent Black Carbon (BC) mass concentration was measured by a 7-wavelength Aethalometer® (Model Magee AE33, Aerosol d.o.o., Slovenia). The photochemical age of the SOA was

evaluated using co-injected deuterated butanol (D9-butanol), which was used as a "photochemical clock" (Barmet et al., 2012) and probed with a quadrupole proton-transfer-reaction mass spectrometer (PTR-MS, Ionicon, Austria). Elemental ratios were measured with a high-resolution time-of-flight aerosol mass spectrometer (AMS, Aerodyne Inc., Billerica, MA, USA). ROS measurements were conducted using an online instrument for particle-bound ROS (OPROSI) (Wragg et al., 2016). Particulate carbon was evaluated by a thermal-optical carbon analyzer (Desert Research Institute Model 2001A, Atmoslytic Inc., Calabasas, CA, USA). Transmission electron microscopy (TEM) images were taken by TEM (JEM-2100F, JEOL Ltd, JP). Chemical SOA composition from filter samples was investigated by direct insertion probe – high-resolution time-of-flight MS (DIP-HRTOFMS; Pegasus® GC-HRT 4D; LECO, St. Joseph, MI, USA) (Käfer et al., 2019), and two-dimensional gas chromatography time-of-flight mass spectrometry (GC × GC-TOFMS; Pegasus® BT 4D GC × GC, LECO, St. Joseph, MI, USA). Particulate carbon was evaluated by a thermal-optical carbon analyzer (Desert Research Institute Model 2001A, Atmoslytic Inc., Calabasas, CA, USA). All methods are described in detail in (Offer et al., 2022) and the SI. Additionally, methanolic extracts of SP-SOA were examined by ultrahigh-resolution Fourier-transform ion cyclotron resonance mass spectrometry (SolariX, 7 T FT-ICR MS, Bruker Daltoniks, Bremen, GE) with electrospray ionization in positive and negative mode as described in the SI.

### 2.3. Cell culture and exposures

The BEAS-2B cell line, an SV-40-transformed human bronchial epithelial cell line (obtained from ATCC, No. CRL 9609), was cultured with BEBM medium along with all the additives (Lonza/Clonetics Corporation, Cologne, GE) except GA-1000 (gentamycin-amphotericin B mix), which was replaced with 100 U $ml^{-1}$ penicillin and 100 μg $ml^{-1}$ streptomycin (P/S; Sigma-Aldrich, GE). Twenty-four mm transwell inserts (0.4 μm pore-size, Corning, NY, USA) precoated with 0.03 mg $ml^{-1}$ bovine collagen Type 1 (Gibco, Dublin, IRL) and 0.01 mg $ml^{-1}$ bovine serum albumin (Sigma-Aldrich, GE) were seeded 4 days prior to the experiments and were kept at 37 °C in humidified air containing 5% $CO_2$.

Cells were exposed in the ALI system (Vitrocell® Automated Exposure Station Standard Version) with complete BEBM medium supplemented with 15 mM N-2-hydroxyethylpiperazine-N-2-ethane sulfonic acid (HEPES) buffer solution (Thermo Fisher Scientific, GE) in the basolateral compartment (Offer et al., 2022). Cells were then exposed for 4 h to the conditioned (85% r.h. 37 °C) undiluted (1:1), and differently diluted aerosols (1:3 and 1:30). These dilutions correspond to ≈ 5.6 and 0.56 ng $cm^{-2}$, respectively, for $SOA_{\beta Pin}$-SP and 9.3 and 0.93 ng $cm^{-2}$, respectively, for $SOA_{Nap}$-SP (Table S1). All experiments represent a single exposure under certain conditions, repeated for at least three independent times. After exposure, the effects of the aerosols on the cells were examined with several assays, and the exposure medium was collected on ice for direct analysis or frozen at −80 °C for further analysis.

### 2.4. Cell viability analysis

The PrestoBlue assay was used to measure cell viability, was performed according to the manufacturer's instructions and is further detailed in the SI section.

### 2.5. RNA extraction, library construction, sequencing and gene expression

Following exposure, the membranes containing the cells were incubated in RNAprotect Cell Reagent (QIAGEN, Hilden, GE) overnight at 4 °C. Then, the membranes were removed, and the cells were stored at −20 °C until the RNA extraction. Total RNA was extracted from the cells using an RNA Plus mini kit (QIAGEN, Hilden, GE) according to the manufacturer's instructions. The quality of the extracted RNA was assessed with a Nanodrop and TapeStation (Agilent Technologies, CA, USA) according to the manufacturer's instructions. Replicates with high RNA integrity (RIN > 9.8) were processed for RNA-Seq at the Crown Genomics Institute of the Nancy and Stephen Grand Israel National Center for Personalized Medicine, Weizmann Institute of Science. Total RNA (500 ng for each sample) was processed using the Inhouse poly A-based RNA-seq protocol (INCPM mRNA Seq). Libraries were evaluated by Qubit (Thermo Fisher Scientific) and TapeStation (Agilent Technologies, CA, USA). Sequencing libraries were constructed with barcodes to allow 45 samples to be multiplexed on two lanes of an Illumina NovaSeq machine using the SP (100 cycles) protocol. The output was ~ 22.9 million single-end 100-bp reads per sample. Fastq files for each sample were generated by the usage bcl2fastq v2.20.0.422.

Gene expression was performed on the extracted RNA using a StepOnePlus Reverse Transcription (RT) PCR instrument (Applied Biosystems, Foster City, CA, USA) as previously described (Pardo et al., 2017) and is further detailed in the SI. Primers were purchased from Sigma-Aldrich, IL) and are described in Table S2.

### 2.6. Bioinformatics analysis

A detailed description of the RNA-seq data analysis and software is provided in the SI section. Differentially expressed genes were determined by a p-adj of < 0.05 and absolute fold changes > 2 and max raw counts > 30. Four replicates were tested for each exposure type. All clean air (CA) samples were grouped together and used for 8 pairwise comparisons against each SP and SOA-SP dilution. Principal component analysis (PCA) and hierarchical clustering (distance: Pearson's dissimilarity, method: Ward.d) were performed based on the 1,000 most variable genes. CA outlier samples E34A2, E35A1 and E37A2 were excluded from the analysis, as these samples were distinctively different from all other CA samples. Unsupervised analysis was executed to explore a pattern of gene expression by clustering the 1,316 genes that were determined to be differentially expressed genes (DEGs). Standardized, log 2 normalized counts were used for the K-Means clustering analysis that was performed with Rstudio v3.6.1.

To determine the most significantly relevant biological functions and pathways, DEGs were analyzed with Ingenuity Pathways Analysis (IPA; QIAGEN, Hilden, GE; Ingenuity® Systems, https://www.ingenuity.com). Fig. S1 shows the pipeline for the analysis.

### 2.7. Cytokine detection

The Luminex® technique was used to detect the cytokine expression profiles in the samples. Cytokines were measured with the Milliplex Magpix instrument (Merck KGaA, Darmstadt, GE) using the MILLIPLEX MAP Human High Sensitivity T Cell Panel-Immunology Multiplex Assay. Eight cytokines were chosen for analysis: CXCL11/I-TAC, IFNγ, IL-12p70, IL-1b, IL-23, IL-6, IL-8 and TNF-α. Analysis was performed according to the manufacturer's instructions. Twenty-five microliters of the cell medium was taken for the analysis. Each cytokine had a calibration curve within the assay; however, the detection range was different for each measured cytokine; CXCL11/I-TAC: 1.46–6000 pg/ml, IFNγ: 0.61–2500 pg/ml, IL-12p70: 0.49–2000 pg/ml, IL-1β: 0.49–2000 pg/ml, IL-23: 7.23–32500 pg/ml, IL-6: 0.18–750 pg/ml, IL-8: 0.31–1250 pg/ml and TNF-α 0.43–1750 pg/ml. Cytokine concentrations were determined by fluorescence intensity. Fluorescence data were analyzed with Millipore Milliplex Analyst version 3.4 according to the manufacturer's recommendations. Statistical analyses were performed with the calculated concentrations of each sample.

### 2.8. Oxidative stress marker, malondialdehyde (MDA) detection

Malondialdehyde (MDA), a marker of lipid peroxidation, was

measured as previously described (Wu et al., 2017), and a further description is found in the SI section.

### 2.9. DNA damage, comet assay

DNA damage was assessed by an alkaline comet assay as previously described (Di Bucchianico et al., 2017) and is further detailed in the SI section.

### 2.10. Statistical analysis

The data for the cell viability, cytokine levels, DNA damage, MDA levels and transcript levels by qPCR are expressed as the means ± standard deviation (SD) representing three independent experiments. Differences between group means were tested by two-way ANOVA with a mixed effect model with a Geisser-Greenhouse correction. Differences were considered significant at a probability level of $p < 0.05$ using Tukey's honestly significant difference (HSD) hypothesis testing. The statistical analysis and the generation of the graphs were performed with GraphPad #9 software (GraphPad Software La Jolla, CA 92037, USA).

## 3. Results

### 3.1. Physical and chemical characterization of $SOA_{\beta Pin}$-SP and $SOA_{Nap}$-SP particles

Both aerosol particles were generated under similar OH exposure ($SOA_{Nap}$-SP: $2.4 \times 10^{11}$ s cm$^{-3}$; $SOA_{\beta Pin}$-SP: $2.5 \times 10^{11}$ s cm$^{-3}$) conditions, equivalent to approximately 3 days of photochemical atmospheric aging. Both SOA had similar elemental carbon (EC) and organic carbon (OC) contents, volatility, size distribution, mass and number concentrations as well as particle shapes (Table S1). TEM imaging revealed that the aerosol particles consisted of collapsed fractal SP agglomerates coated by organic matter from condensation of secondary organic material from the photooxidation of the naphthalene and β-pinene precursors in the PAM chamber. The calculated aerosol particle deposition was 1.6-fold higher for $SOA_{Nap}$-SP (9.3 ng cm$^{-2}$) than for $SOA_{\beta Pin}$-SP (5.6 ng cm$^{-2}$) (Table S1).

Untargeted mass spectrometric analyses reveal that in contrast to similar physical properties, the two SOA types differ in chemical composition. At a signal-to-noise ratio of > 1000, two-dimensional gas chromatography time-of-flight mass spectrometry (2-D GC TOF MS) with electron ionization detected 798 and 397 peaks for $SOA_{\beta Pin}$-SP and $SOA_{Nap}$-SP, respectively. $SOA_{\beta Pin}$-SP was dominated by aliphatic semi-volatile organic compounds, with nopinone the major oxidation product from β-pinene. The cyclic structures identified in $SOA_{\beta Pin}$-SP indicate the presence of bicyclic carbon backbone of β-pinene (e.g. angelicoidenol) or of monocyclic oxygenated cyclohexane (e.g., cyclohexadione), lactones (e.g., 6-methyl-3,4-dihydro-2H-pyran-2-one) and furans (e.g. 2,3-dihydro-4-(1-methylpropyl)-furan). The photooxidation products in $SOA_{Nap}$-SP retained one or both aromatic rings, leading to oxygenated naphthalenes (e.g., dihydroxynaphthalene), naphthoquinones and aromatic lactones as well as benzenes with oxygenated substituents (e.g., 1,2-benzenedicarboxaldehyde). In both SOA types, polyunsaturated hydrocarbons and oxygenated hydrocarbons were detected in small amounts. These compounds may be assigned to primary emissions of the combustion aerosol standard (CAST) or evolve from thermal decomposition of nonrefractory SOA constituents (Claflin and Ziemann 2019; Zhao et al., 2020).

Aerosol particle constituents of lower volatility were analyzed on-line by aerosol mass spectrometry (AMS) and off-line by direct inlet probe mass spectrometry (DIP-MS). The AMS results showed higher O:C and lower H:C for $SOA_{Nap}$-SP than for $SOA_{\beta Pin}$-SP, which is consistent with the higher oxidative potential of $SOA_{Nap}$-SP measured by the On-line Particle-bound Reactive Oxygen Species Instrument (OPROSI) (Zhang et al., 2022). Both, AMS and DIP-MS analyses indicate the abundance of oxygenated aerosol particle constituents in the high-molecular weight fraction, based on thermal fragments. The molecular composition of the high-molecular weight fraction was further explored by ultrahigh resolution mass spectrometry (UHR-MS) with electrospray ionization (ESI) in both positive (+ESI) and negative mode (-ESI) and is further detailed in the SI.

The + ESI mass spectrum of $SOA_{\beta Pin}$-SP contain high-molecular weight species with up to 20 oxygen atoms and distinct Gaussian-like distributions of peak intensities centered at approximately $m/z$ 410, 610 and 785 (Fig. 1A). Within each distribution, 14 or 16 amu peak distances indicate homolog series with [–$CH_2$-] or [-O-] entities, respectively. Such a mass spectrometric pattern has been previously linked to oligomeric structures formed during photooxidation of SOA precursors (Kalberer et al., 2004), particularly dimers from β-pinene photooxidation (Kenseth et al., 2018). The presence of oligomers was also verified by collision-induced dissociation of the primary ions, which retained the overall mass spectrometric pattern (Fig. S2). Hence, the assigned oligomers were not an artifact from ionization. A plot of the carbon number (#C) vs. the average carbon oxidation state ($OS_C$) (Kroll et al., 2011) highlights the oligomers and reveals major peak intensities that appeared at multiples of 10 carbon atoms, which is equal to the number carbons in β-pinene ($C_{10}H_{16}$), and leveled off at 60 carbon atoms (Fig. 1B). $SOA_{\beta Pin}$-SP has an $OS_C$ of −0.9, which was derived from an O:C of 0.38 and an H:C of 1.66 and does not differ significantly between dimers and hexamers. However, SOAs from monomers of β-pinene have a higher $OS_C$ of −0.35, which can be observed for compounds with a maximum of 10 carbon atoms. A representative chemical structure based on elemental ratios of $SOA_{\beta Pin}$-SP may be given by diaterpenylic acid acetate ($C_{10}H_{16}O_4$), which is a known photooxidation product of monoterpenes (Claeys et al., 2009), and its oligomers.

$SOA_{Nap}$-SP also features Gaussian-like peak intensity distributions in the + ESI mass spectrum around $m/z$ 240 and 420, but with highest intensities for monomers (Fig. 1C), which agrees with findings from Wang et al., (2018). In the #C vs. $OS_C$ space, the $SOA_{Nap}$-SP oligomers appear with multiples of 10 carbon atoms end with tetramers at #C of 40 as naphthalene ($C_{10}H_8$) also contain 10 carbon atoms (Fig. 1D). Similar to $SOA_{\beta Pin}$-SP, the $OS_C$ of the oligomers of $SOA_{Nap}$-SP remain stable, but increase from the dimer ($OS_C$ of −0.18) to the monomer (-$OS_C$ of 0.09). Based on the average elemental ratios (O:C: 0.44; H:C: 1.07), a representative structure of $SOA_{Nap}$-SP may be given by ferulic acid or dimethyl phthalate ($C_{10}H_{10}O_4$) as well as its oligomers (Claeys et al., 2009; Ng et al., 2011). The exemplary structures for $SOA_{\beta Pin}$-SP and $SOA_{Nap}$-SP also illustrate the fundamental difference in aromaticity between the two SOA-SPs, which can be generalized by the concept of the aromaticity index (AI; $AI_{aromatics} \geq 0.5$) (Koch and Dittmar 2006). For $SOA_{\beta Pin}$-SP<1% of the total peak intensity belongs to aromatic compounds, which account for 26% of the total peak intensity in $SOA_{Nap}$-SP.

The -ESI mass spectra reveal a strong dominance of the dimers for both aerosol types and a high aromaticity for $SOA_{Nap}$-SP (32% of total peak intensity from aromatic compounds). More information about -ESI analysis and an overview of chemical aerosol properties is detailed in the SI (Fig. S3 and Table S3). Additional information about the physical and chemical properties of the particles can be found in Offer et al. (2022).

### 3.2. Cytotoxicity of SP, $SOA_{\beta Pin}$-SP or $SOA_{Nap}$-SP

The toxicity of SOA-SP was determined by measuring the metabolic activity with Prestoblue, a resazurin-based solution. Exposure was performed to $SOA_{\beta Pin}$-SP or $SOA_{Nap}$-SP versus the control groups that were exposed to either uncoated SP or clean air (CA). Exposure of BEAS-2B cells to $SOA_{Nap}$-SP led to a significant reduction in metabolic activity, particularly under undiluted (1:1) conditions (40%) and at a dilution of 1:3 (30%). Exposure to $SOA_{\beta Pin}$-SP did not reduce the metabolic activity compared to SP for all dilutions tested (reduction of 10–15% for both the $SOA_{\beta Pin}$-SP and SP, compared to CA, respectively) (Fig. 2), suggesting an increased toxic response for $SOA_{Nap}$-SP compared to $SOA_{\beta Pin}$-SP.

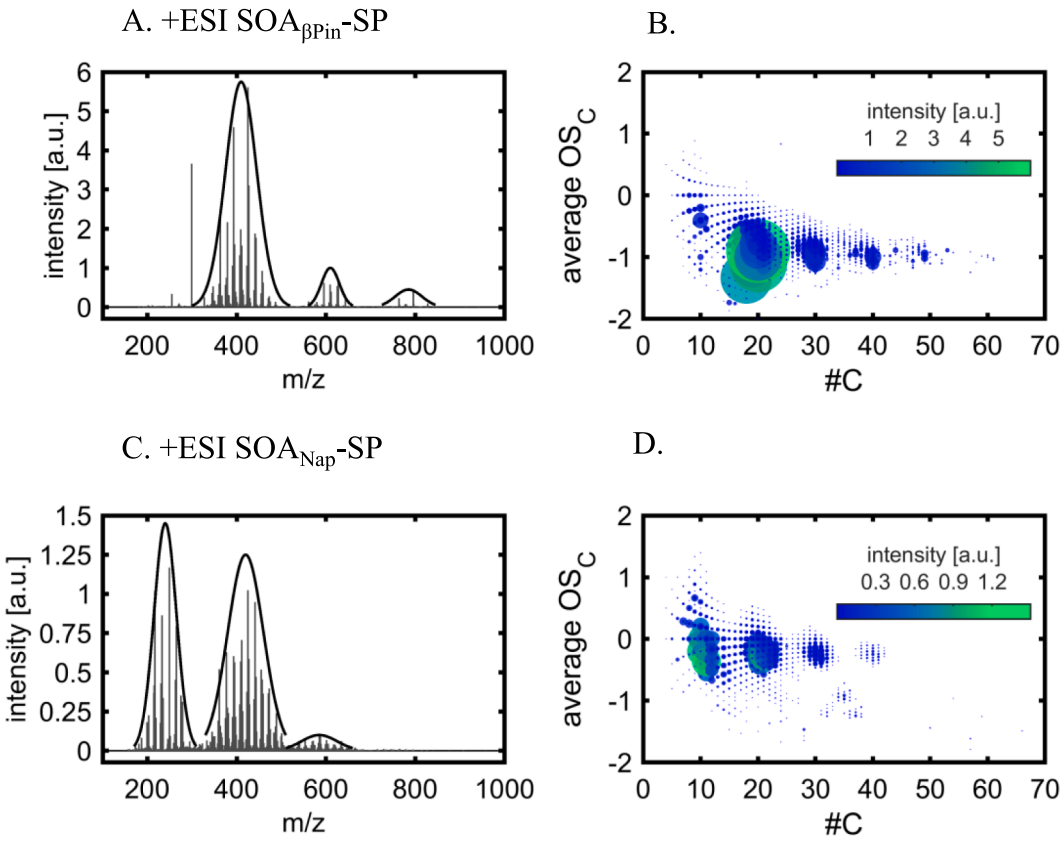


**Fig. 1.** +ESI mass spectra of methanol extracts with carbon number (#C) vs. average carbon oxidation state ($OS_C$) for $SOA_{\beta Pin}$-SP (A and B) and $SOA_{Nap}$-SP (C and D). Black solid lines highlight the peak distribution of oligomeric structures in the mass spectra.

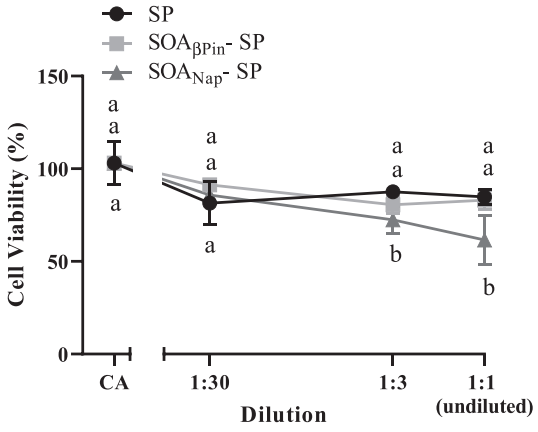


**Fig. 2.** Cell viability following soot particle (SP) and SP coated by SOA (SOA-SP) exposure. BEAS-2B cells were exposed in the ALI for 4 h to different dilutions of SP, SP coated by β-pinene photooxidation products ($SOA_{\beta Pin}$-SP) or SP coated by naphthalene photooxidation products ($SOA_{Nap}$-SP). The data represent *n* independent experiments with one technical replicate, normalized to the control (cells exposed to clean air, CA), SP, $n = 3$, $SOA_{\beta Pin}$-SP, $n = 4$, $SOA_{Nap}$-SP, $n = 4$, for all dilutions, and CA, $n = 8$. Data are expressed as the mean ± SD. Two-way ANOVA was used for the analysis. Means with different letters are significantly different. Differences were considered significant at a probability level of $^*p < 0.05$ using Tukey's honestly significant difference (HSD) hypothesis testing.

### 3.3. Genome-wide transcriptional responses to $SOA_{\beta Pin}$-SP or $SOA_{Nap}$-SP

RNA-Seq was performed to detect differential gene expression in BEAS-2B cells exposed to $SOA_{\beta Pin}$-SP or $SOA_{Nap}$-SP versus the control groups. Since the PrestoBlue assay indicated not>40% impairment of cell viability after 4 h of exposure to the 1:30 and 1:3 dilutions, RNA-seq of samples exposed to these two dilutions represent actual transcript changes.

Data on the expression of 16,968 genes were retained for the RNA-Seq analysis. PCA, based on the most variable genes, showed the largest separation between the CA samples and SOA-SP for the two tested dilutions (Fig. 3).

#### 3.3.1. Differential gene expression from SOAs-SP

The comparisons performed were between the SP dilution 1:3 and all CA samples (SP3vsCA), $SOA_{\beta Pin}$-SP dilution 1:3 and all CA samples ($SOA_{\beta Pin}$-SP3vsCA), and between $SOA_{Nap}$-SP dilutions 1:3 ($SOA_{Nap}$-SP3vsCA). In addition, we used the same groups for comparison with a dilution of 1:30, namely, SP30vsCA, $SOA_{\beta Pin}$-SP30vsCA and $SOA_{Nap}$-SP30vsCA. The analysis yielded 671 DEGs for SP3vsCA (479 upregulated and 192 downregulated), 725 DEGs for $SOA_{\beta Pin}$-SP3vsCA (441 upregulated and 284 downregulated) and 986 DEGs for $SOA_{Nap}$-SP3vsCA (624 upregulated and 362 downregulated). Additionally, 409 DEG for SP30vsCA (322 upregulated and 87 downregulated), 288 DEG for $SOA_{\beta Pin}$-SP30vsCA (231 upregulated and 57 downregulated) and 673 DEGs for $SOA_{Nap}$-SP30vsCA (491 upregulated and 182 downregulated) (Fig. S4 and Fig. S5). The RNA-seq analysis focused on the differences at a dilution of 1:3 as fewer DEGs were observed for SP and $SOA_{\beta Pin}$–SP than for $SOA_{Nap}$-SP at dilutions of 1:30 and 1:3, respectively. In addition, the cell viability assay showed little biological response at a dilution of 1:30 that was thereafter supported with other biological assays.

DEG were analyzed by two approaches. The first approach was used to observe changes at the individual gene level, whereas the second approach was used to obtain a comprehensive overview of groups of genes and their relevant altered pathways.

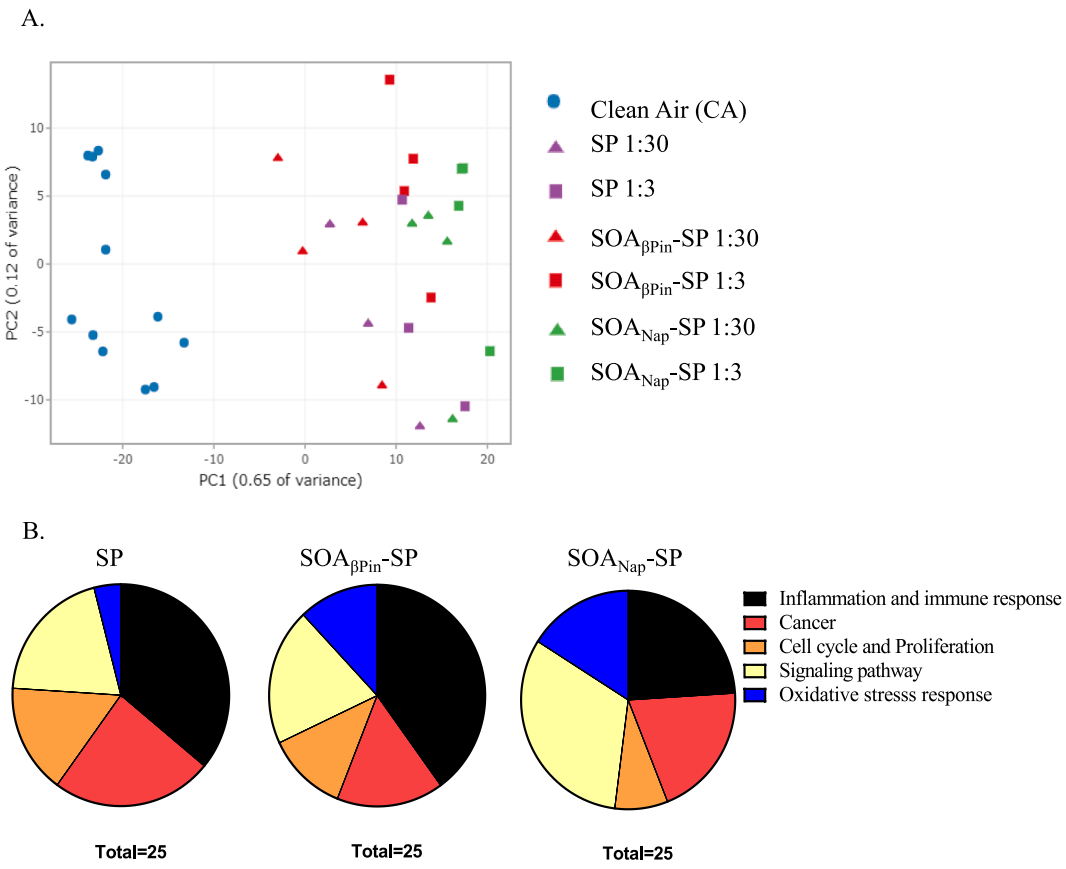


**Fig. 3.** Principal component analysis (PCA) plot of RNA-Seq data and canonical pathway grouping after exposure to SP or SOA-SP. (A) Purple color indicates exposure to SP, red symbols indicate exposure to SOA$_{\beta Pin}$-SP, green symbols indicate exposure to SOA$_{Nap}$-SP, blue symbols and round shapes indicate exposure to clean air (CA). Triangle shapes indicate a dilution of 1:30, and square shapes indicate a dilution of 1:3. (B) The top 25 canonical pathways used for this analysis were grouped according to their function and cell responses; "Inflammation and/immune response", "Cancer", "Cell cycle and proliferation", "Signaling pathway" and "Oxidative stress response", further description about the canonical pathway grouping strategy is detailed in the SI. The pie charts demonstrate the relative contribution of the major groups. IPA filters were set to p-adj of $< 0.05$, absolute fold changes $> 2$ and max raw counts $> 30$ for enriched canonical pathways.

### 3.3.2. *Individual unbiased gene analysis*

To visualize and assess the transcriptional changes at the gene level, Venn diagrams (Fig. S4) and volcano plots (Fig. S5) were plotted (Koch et al., 2018). The expression of 15 most significant up- and down-regulated individual genes is presented in Table S4. Among the SP, SOA$_{\beta Pin}$-SP, and SOA$_{Nap}$-SP groups, common highly expressed individual transcription factors were found. These include FOSB, which is part of the activator protein (AP-1) transcription factor complex, and transcription factor Grainyhead-like 3 (GRHL3), which is related to the regulation of phosphatase tensin homolog (PTEN) and the phosphatidylinositol 3-kinases (PI3K)/protein kinase B (AKT)/mechanistic target of rapamycin (mTOR) signaling pathway. Other highly expressed genes are the redox-sensitive *HMOX-1* and *RasD2* genes. For the upregulated genes, no special trends were identified between the SP, SOA$_{\beta Pin}$-SP, and SOA$_{Nap}$-SP groups. However, in specific genes, that were mutual for the SP, SOA$_{\beta Pin}$-SP, and SOA$_{Nap}$-SP groups, SOA$_{Nap}$-SP induced higher gene expression levels than SP and SOA$_{\beta Pin}$-SP. The number of "down-regulated" genes was small for the SP, SOA$_{\beta Pin}$-SP, and SOA$_{Nap}$-SP groups. The greatest reduction in gene levels was recorded for SOA$_{Nap}$-SP and SOA$_{\beta Pin}$-SP compared to SP. Among the downregulated genes in SOA$_{Nap}$-SP, a reduction in the level of alcohol dehydrogenase 1B (*ADH1B*) that is responsible for the metabolism of a wide variety of substrates, including ethanol, aliphatic alcohols, and lipid peroxidation products (Table S4).

### 3.3.3. *Pathway analysis*

To obtain a comprehensive insight into the biological functions and pathways influenced by exposure to SOA$_{\beta Pin}$-SP or SOA$_{Nap}$-SP in lung cells, clustering (Fig. S6) and functional annotation of DEGs were performed using Ingenuity Pathway Analysis (IPA). In the identified pathways, differential expression of genes significantly exceeded a p-value in at least one experimental setting and the activating z-score threshold was surpassed to determine the activation or inhibition of pathways.

Using IPA, each SOA-SP was analyzed separately compared to the CA samples, and relevant canonical pathways were identified. SOA$_{\beta Pin}$-SP and SOA$_{Nap}$-SP show common *canonical pathways* related to the inflammatory response, stress response and MAPK signaling. A detailed description of the z score canonical pathway, upstream analysis, disease and function information, and validation by real-time PCR (*HMOX-1, Bcl2, IL-8, GADD45, AhR, MMP-3* and *MMP-10*) (Fig. S7) is presented in the SI.

Twenty-five canonical pathways are summarized as pie charts based on their known involvement in various cell responses. The canonical pathway groups were defined as i) "Inflammation and/immune response" (ii) "Cancer" (iii) "Cell cycle and proliferation" (iv) "Signaling pathway" and (v) "Oxidative stress response". While some pathways may be related to more than one group or cluster, the same classification was kept throughout the analysis to highlight the general changes in the activated pathways by the exposure to the different particle types (Table S5). The relative contribution of the canonical pathway of human lung cells exposed to SP and SOA-SP showed that a large portion of the pathways were related to the "inflammatory/immune response" (Fig. 3B and Table S5). These pathways largely consist cells exposed to SP and SOA$_{\beta Pin}$-SP. The "Signaling pathway", related to "MAP kinase signaling",

was more prevalent in cells exposed to $SOA_{Nap}$-SP. Exposure to both $SOA_{\beta Pin}$-SP and $SOA_{Nap}$-SP increased the contribution of the "oxidative stress response" in comparison to SP. No substantial difference was observed for the "Cell cycle and proliferation" and "Cancer" pathways among SP, $SOA_{\beta Pin}$-SP and $SOA_{Nap}$-SP exposures.

### 3.4. Expression of proinflammatory cytokines in cells exposed to SOA-SP

Eight cytokines (IL-6, IL-8, IL-1β, TNF-α, IL-12p70, IFNγ, CXCL11/I-TAC, and IL-23) were analyzed from the medium of the exposed cells to assess the induction of inflammatory response by SOA-SP. These cytokines were identified based on the RNA-seq analysis, but have also been shown to increase in response to PM exposure in human bronchial epithelial cells in previous studies (Das et al., 2021; Longhin et al., 2018). Changes in cytokine secretion levels during exposure to different dilutions of SOA-SP were investigated (Fig. 4). Cytokine levels showed dose-dependent response when exposed to SOA-SP compared to that of the controls (SP and CA) for most cytokines tested, further demonstrating the importance of SOA in generating the inflammatory response. The dilution effect was observed with up to a 1:3 dilution, which avoided significant cell death compared to that of the undiluted levels. Lower levels of cytokines expression was observed in SP than SOA-SP. The expression levels of IL-6 and IL-8 were significantly higher in SOA-SP than in SP at a dilution of 1:3. No significant differences between $SOA_{\beta Pin}$-SP and $SOA_{Nap}$-SP were observed for IL-6, IL-8 or IL-1β.

The expression of TNF-α, IL-12, IFN-γ, CXCL11/I-TAC, and IL-23 was significantly higher in cells exposed to $SOA_{Nap}$-SP than in cells exposed to $SOA_{\beta Pin}$-SP at a dilution of 1:3. The secretion of IL-8, IL-1β, IL-12, IFN-γ, and IL-23 significantly increased in a dose-dependent manner when cells were exposed to $SOA_{\beta Pin}$-SP and $SOA_{Nap}$-SP, especially for the $SOA_{Nap}$-SP at a dilution of 1:3.

### 3.5. Exposure to SOA-SP induces oxidative stress and damage in lung cells

Pathway analysis revealed that exposure to $SOA_{\beta Pin}$-SP and $SOA_{Nap}$-SP are associated with expression of genes related to Nrf2- mediated oxidative stress response, suggesting that the oxidative stress response and subsequent DNA damage may be important mechanisms leading to the adverse biological effects induced by exposure to SOA. Some of the genes related to Nrf-2 mediated oxidative stress response were evaluated by real-time PCR after exposure to SOA-SP. Exposure to SOA-SP showed a statistically significant increase in *HMOX-1* and Glutamate-cysteine ligase regulatory subunit (*GCLM)* gene levels compared to that of SP. Whereas NAD(P)H dehydrogenase (quinone 1) (*NQO-1)* transcript level increased in $SOA_{Nap}$-SP and not $SOA_{\beta Pin}$-SP. No change was evident in

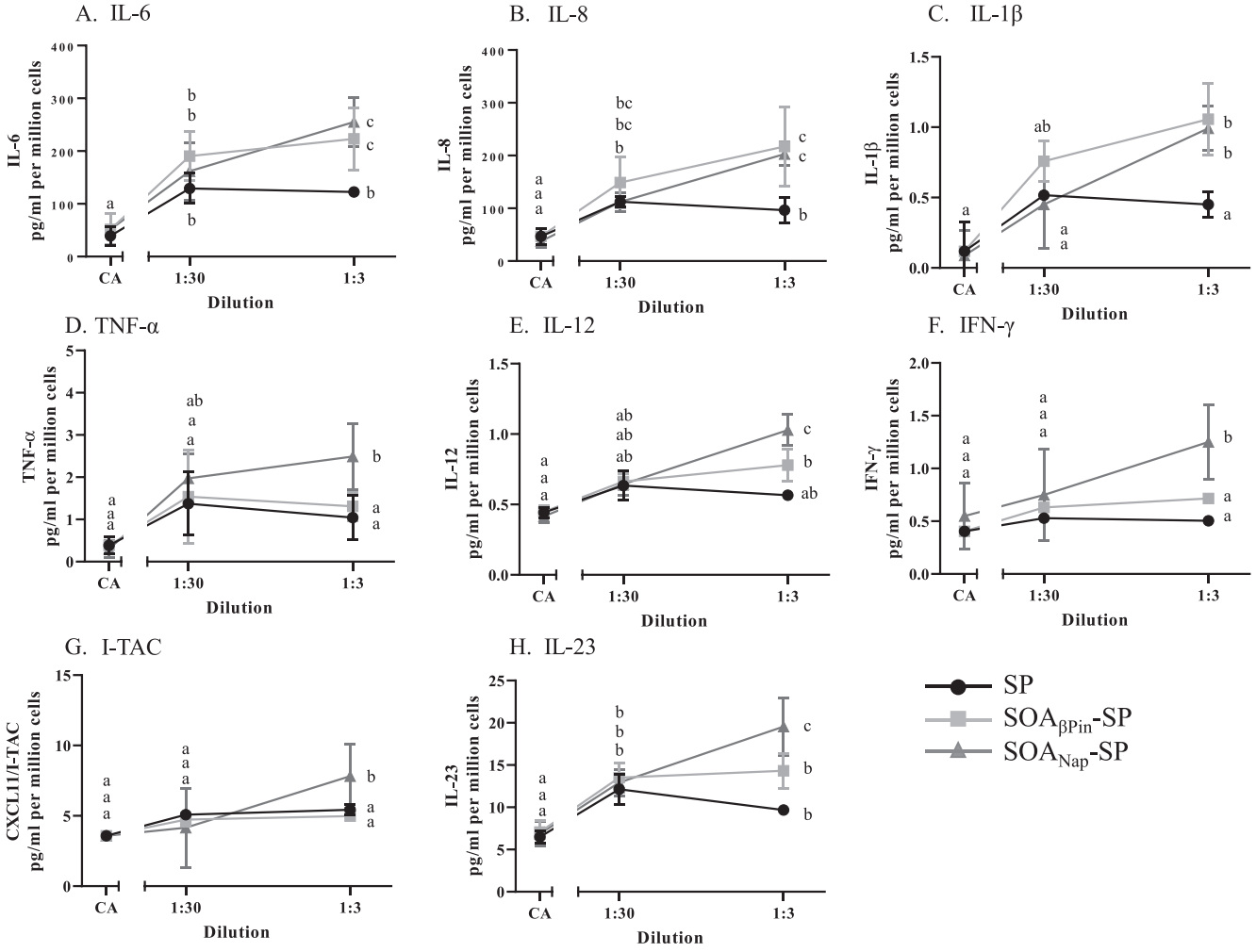


**Fig. 4.** Cytokine expression after exposure to SP and SOA-SP. BEAS-2B cells were exposed for 4 h to 1:3 and 1:30 dilutions of SP, $SOA_{\beta Pin}$-SP or $SOA_{Nap}$-SP and CA. Cytokine levels were detected in the basolateral medium. (A) IL-6, (B) IL-8, (C) IL-1β, (D) TNF-α, (E) IL-12, (F) IFN-γ, (G) CXCL11, and (H) IL-23. The data represent *n* independent experiments with one technical replicate, compared to cells exposed to CA, SP, $n = 3$, $SOA_{\beta Pin}$-SP, $n = 4$, $SOA_{Nap}$-SP, $n = 4$, for all dilutions, and CA, $n = 8$. Two-way ANOVA was used for the analysis. Means with different letters are significantly different. Differences were considered significant at a probability level of $^{*}p < 0.05$ using Tukey's HSD hypothesis testing.

the Glutamate—cysteine ligase catalytic subunit (*GCLC)* and (Fig. 5A-D). To explore the oxidative stress response, MDA levels were measured after exposure to $SOA_{\beta Pin}$-SP and $SOA_{Nap}$-SP. After exposure to 1:3 dilution $SOA_{Nap}$-SP, BEAS-2B cells showed a significant increase in MDA levels. Conversely, no change in MDA levels was recorded following exposure to $SOA_{\beta Pin}$-SP and SP at any dilution tested (Fig. 5E).

ROS can damage DNA and lead to genotoxicity and DNA instability (Bai et al., 2017). A comet assay was performed to assess DNA lesions and genomic instability following exposure to $SOA_{\beta Pin}$-SP and $SOA_{Nap}$-SP. $SOA_{Nap}$-SP showed a statistically significant increase in the percentage of DNA in the tail at 1:30 and 1:3 dilutions compared to that of the control cells. No change was observed for $SOA_{\beta Pin}$-SP and SP compared to the control (Fig. 5F). This implies a stronger genotoxicity response is induced by $SOA_{Nap}$-SP than by $SOA_{\beta Pin}$-SP.

Activation of oxidative stress signaling by aryl hydrocarbon receptor (AhR) and induction of the related Cytochrome P450 (Cyp) enzymes (Pardo et al., 2020) were evaluated by real-time PCR after exposure to SOA-SP, as AhR can be directly activated by PAH (Pardo et al., 2020). Exposure to $SOA_{Nap}$-SP showed a statistically significant increase in *AhR* and *cyp1a1* gene levels compared to that of $SOA_{\beta Pin}$-SP. No change was evident in the *cyp1b1* and aldehyde dehydrogenase (*ALDH*) genes in SOA-SP (Fig. 6), suggesting that the $SOA_{Nap}$-SP obtains Cyp-specific response and is driven by PAH.

## 4. Discussion

SOA from biogenic and anthropogenic sources account for a substantial fraction of the total PM exposure (Borbon et al., 2013; Chowdhury et al., 2019; Chowdhury et al., 2018; Eaves et al., 2020; Gu et al., 2021; Guenther et al., 1995; Han et al., 2020; Ito et al., 2019; Tuet et al., 2017a), and can induce adverse health effects upon exposure (Chowdhury et al., 2019; Chowdhury et al., 2018; Eaves et al., 2020; Han et al., 2020; Ito et al., 2019; Khan et al., 2021; Tuet et al., 2017a). It was estimated that the mass per surface area from human inhalation representing realistic conditions or worst case exposure conditions are 0.03 ng $cm^{-2}$ $h^{-1}$ and 5 ng $cm^{-2}$ $h^{-1}$ (Paur et al., 2011). In this study, the calculated particle mass concentration (dilution 1:3) per hour was 1.4 and 2.2 ng $cm^{-2}h^{-1}$ for $SOA_{\beta Pin}$-SP and $SOA_{Nap}$-SP, respectively, corresponding to average levels of ambient exposure conditions. Thus, the lung cells were exposed to two different SOA types with comparable

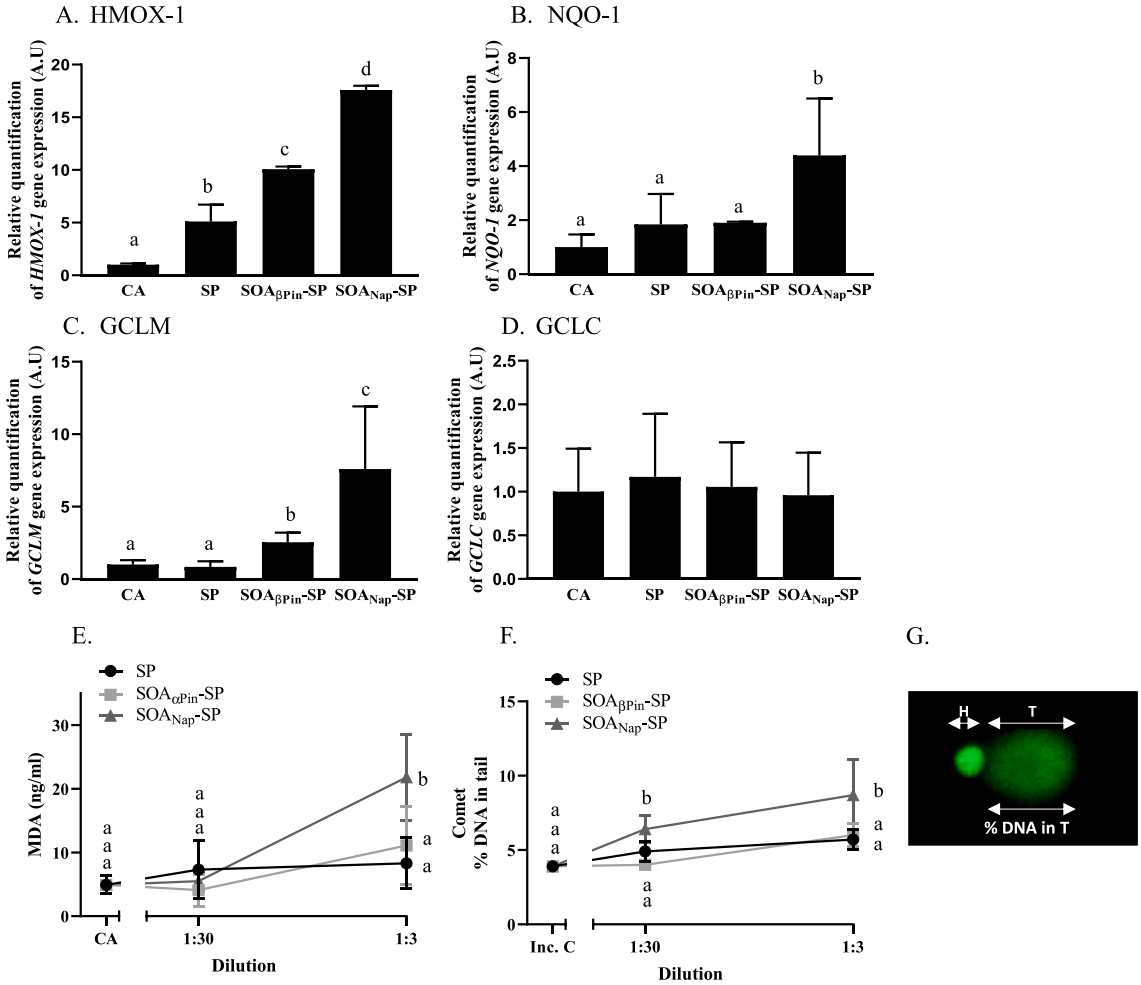


**Fig. 5.** Transcript levels of Nrf-2 related genes, oxidative stress and DNA damage induced by SP and SOA-SP. BEAS-2B cells were exposed for 4 h to 1:3 and 1:30 dilutions of SP, $SOA_{\beta Pin}$-SP or $SOA_{Nap}$-SP and CA. Transcript levels at dilution 1:3 of (A) *HMOX-1*, (B) *NQO-1*, (C) *GCLM* and (D) *GCLC* were analyzed by real-time PCR, and β-Actin was used as an endogenous control. The data represent *n* independent experiments with one technical replicate normalized to cells exposed to CA, SP, $n = 3$, $SOA_{\beta Pin}$-SP, $n = 4$, $SOA_{Nap}$-SP, $n = 4$, and CA, $n = 8$. (E) MDA levels. The data represent *n* independent experiments with one technical replicate compared to cells exposed to CA, SP, $n = 3$, $SOA_{\beta Pin}$-SP, $n = 3$, $SOA_{Nap}$-SP, $n = 4$, for all dilutions, and CA, $n = 7$. (F) Quantitation of %DNA in the tail from dilutions of 1:30 and 1:3 and incubator control (Inc. C) after exposure to the SP and SOA-SP. The data represent *n* independent experiments with one technical replicate compared to cells exposed in the incubator control, SP, $n = 3$, $SOA_{\beta Pin}$-SP, $n = 4$, $SOA_{Nap}$-SP, $n = 5$ for all dilutions and Inc. C, $n = 3$). Two-way ANOVA was used for the analysis. Means with different letters are significantly different. Differences were considered significant at a probability level of $p < 0.05$ using Tukey's honestly significant difference (HSD) hypothesis testing. (G) Representative nucleotides of micro gel comet assay H, head; T, tail.

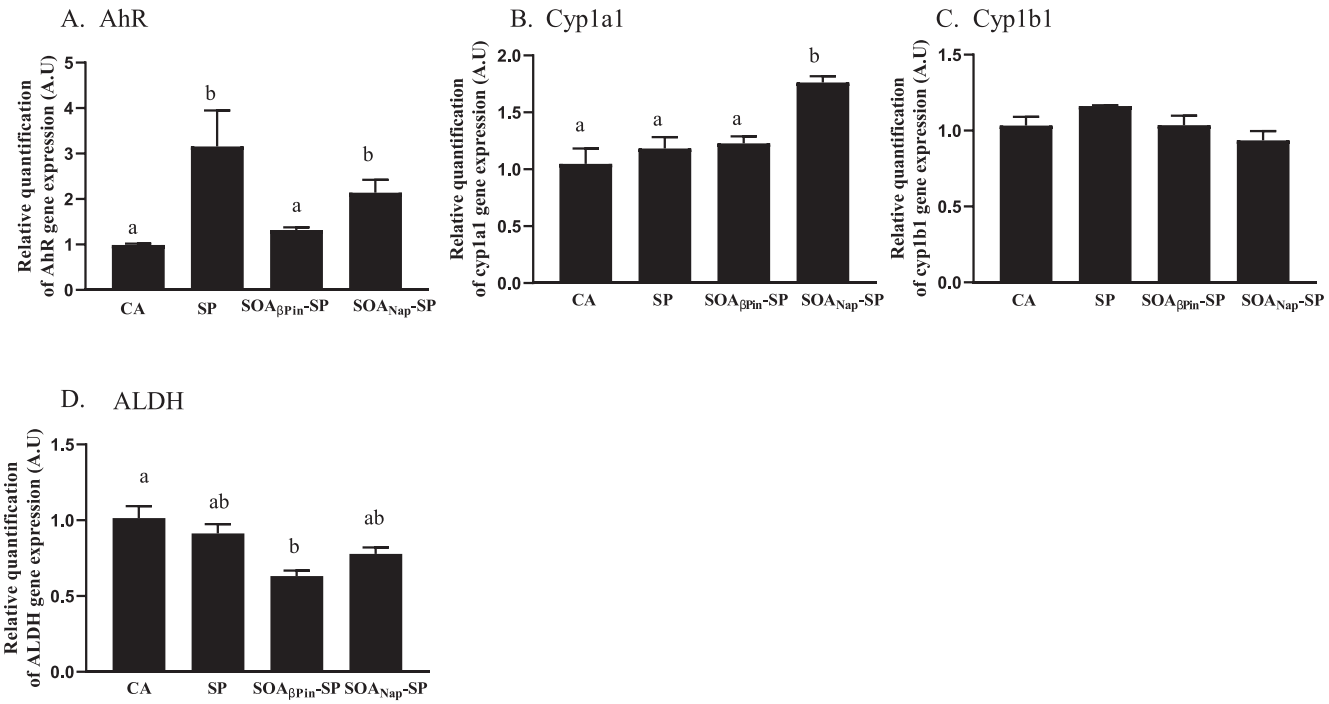


**Fig. 6.** Transcript levels of the AhR-dependent Cyp response after exposure to SP and SOA-SP. BEAS-2B cells were exposed for 4 h to a 1:3 dilution of SP, $SOA_{\beta Pin}$-SP or $SOA_{Nap}$-SP. Transcript levels of (A) *AhR*, (B) *Cyp1a1*, (C) *Cyp1b1* and (D) *ALDH* were analyzed by real-time PCR, and β-Actin was used as an endogenous control. The data represent *n* independent experiments with one technical replicate normalized to cells exposed to CA, SP, $n = 3$, $SOA_{\beta Pin}$-SP, $n = 4$, $SOA_{Nap}$-SP, $n = 4$, and CA, $n = 8$. The data represent mean ± SD. One-way Anova was used for the analysis. Means with different letters were determined to be significantly different at $p < 0.05$ using the Tukey HSD test.

concentrations and similar physical properties, yet, with fundamentally different chemical compositions. The dose in this study was even lower than that in the previous studies using the ALI system, in which lung cells were exposed to 67 ng $cm^{-2}$ proxies of isoprene SOA (Arashiro et al., 2016) or approximately 10 μg $cm^{-2}$ proxies of naphthalene or α-pinene (Chowdhury et al., 2019). However these levels are more representative of the new WHO guidelines (World Health 2021). Nevertheless, comparing exposure parameters to similar studies using SOA followed by in vitro cytotoxicity is complicated as these studies used different exposure systems such as ALI or extracts, as well as various SOA sources with different masses and deposition efficiencies.

Recent studies have focused on the biological effects of PM from various sources and the relation of these effects to adverse health outcomes (Bai et al., 2017; Burnett et al., 2018; Cohen et al., 2017; De Grove et al., 2018; Shi et al., 2021). Due to the high abundance of atmospheric secondary aerosols, several studies have investigated the cytotoxic effects of exposure to biogenic or anthropogenic SOA toward lung cells (Chowdhury et al., 2019; Chowdhury et al., 2018; Eaves et al., 2020; Han et al., 2020; Ito et al., 2019; Tuet et al., 2017a). In the present study, we investigated the cytotoxicity and signaling mechanisms, and identified different pathways induced by SOA exposure from proxies for biogenic ($SOA_{\beta Pin}$-SP) versus anthropogenic ($SOA_{Nap}$-SP) precursors. The physical properties of these SOAs are rather similar (size distribution, volatility, particle shape etc.), but they differ in their chemical nature: $SOA_{\beta Pin}$-SP is less oxygenated and contains mostly structural increments of the terpene backbone with acid and carbonyl functional groups, while $SOA_{Nap}$-SP is more oxygenated and often retains aromatic rings, which is reminiscent of the naphthalene precursor. Both SOA types contain oligomers, but $SOA_{\beta Pin}$-SP contains a larger amount of oligomers that are higher and beyond trimers compared to that of $SOA_{Nap}$-SP. Here we discuss the chemical differences between the two SOA types that contribute to differential biological responses following exposure to BEAS-2B cells.

### 4.1. Signaling mechanism following exposure to SOA

To identify the biological functions and signaling pathways activated by SOA exposure in lung cells, we analyzed and compared genome-wide transcriptome responses after exposing BEAS-2B lung epithelial cells to $SOA_{\beta Pin}$-SP and $SOA_{Nap}$-SP. In this study, both $SOA_{\beta Pin}$-SP and $SOA_{Nap}$-SP induced an increased in the genes related to Nrf2 oxidative stress response, particularly $SOA_{Nap}$-SP. In addition, canonical pathway grouping showed that both $SOA_{\beta Pin}$-SP and $SOA_{Nap}$-SP led to an increased abundance in the "oxidative stress response". The overall profile of the activated biological functions influenced by $SOA_{\beta Pin}$-SP and $SOA_{Nap}$-SP is consistent with the previously reported responses in BEAS-2B cells. A recent study showed that proteome-wide effects of naphthalene-derived SOA significantly upregulated Nrf2-regulated proteins (e.g., NQO1) in BEAS-2B cells (Han et al., 2020). Other SOA types also alter oxidative stress genes: isoprene-derived SOA was shown to alter microRNA (miRNA) expression related to oxidative stress in BEAS-2B cells (Eaves et al., 2020) as well as the induction of the Nrf2 transcription factor and its related genes (Lin et al., 2017). These findings support the notion that SOA is involved in the oxidative stress response, specifically by inducing Nrf2 signaling.

Multiple biological and signaling transduction pathways can be triggered by oxidative stress and particle toxicity (Ahmed et al., 2019; Zheng et al., 2017). For example, exposure to dimethyl selenide (DMSe) aerosols induced elevated genotoxicity, DNA damage, mitogen-activated protein kinases (MAPK) and p53-mediated stress responses, as well as downregulated cholesterol biosynthesis, glycolysis, and interleukin IL-4/IL-13 signaling (Ahmed et al., 2019). Exposing BEAS-2B to ambient SOA promoted the PI3K-Akt, JAK-STAT and FGF/FGFR/MAPK/VEGF signaling pathways, which led to apoptosis and sustained angiogenesis and affected cell proliferation, and these are all important hallmarks of cancer (Zheng et al., 2017). In our study, the induction of MAPK/growth factor-regulated extracellular signal-related kinase (ERK) signaling was detected. These MAPKs (ERKs, JNKs, or p38 MAPKs) are

serine-threonine protein kinases that are activated by high ROS levels and play a major role in oxidative stress signal transduction (Son et al., 2011). It was also found that organics from fine particles (OC, PAHs) (Zheng et al., 2017) and AhR activation (Shi et al., 2021) engage in crosstalk with MAPK signal transductions pathways. Therefore, these observations suggest that the $SOA_{Nap}$-SP signaling cascade is influenced by ROS generation (Zhang et al., 2022) and AhR activation, which was also evident in our study. The higher response to $SOA_{Nap}$-SP exposure is hence attributed to the aromatic moieties identified by the mass spectrometric analysis in this SOA.

Both the individual gene analysis and the pathway analysis showed increase in the transcript levels of matrix metalloproteinase (*MMP*). These MMPs play critical roles in matrix remodeling and modulation of inflammation, cell signaling and intracellular pathways (Dagouassat et al., 2012). Several previous studies have shown a connection between PM chemical composition and the involvement of different types of MMP (Campen et al., 2010; Dagouassat et al., 2012; Xing et al., 2021); for example, *MMP-9* mRNA expression and activity in the aorta were detected in mice exposed to SOA from whole combustion emissions of gasoline and diesel (Campen et al., 2010). It was shown that mice exposed to $PM_{2.5}$ suspension by oropharyngeal aspiration had increased mRNA levels of MMP-2 and MMP-9 in the heart tissue, and PAHs positively correlated with MMP-9 expression (Xing et al., 2021). Our data show that $SOA_{\beta Pin}$-SP and $SOA_{Nap}$-SP mainly increased MMP-1, MMP-3 and MMP-10, whereas a higher effect was induced by $SOA_{Nap}$-SP than $SOA_{\beta Pin}$-SP. This finding is very interesting, as to the best of our knowledge, this is the first time that elevation of these subtypes of MMP have been reported with exposure to SOA. MMP-3 and MMP-10 are secreted from the cells as inactive proMMPs, but they are then activated on the cell surface. These MMPs correlate with respiratory pathologies (Cui et al., 2017); MMP-3 may be involved in the development of lung cancer among chronic obstructive pulmonary disease (COPD) subjects (Brzóska et al., 2014), and MMP-10 is associated with airway inflammation (Kuo et al., 2019). Further studies are therefore needed to better understand the implications of MMP activation in health effects associated with exposure to SOA.

### 4.2. Inflammatory response after exposure to SOA

An increasing amount of evidence points to the involvement of SOA in the inflammatory-related cascade, oxidative stress, and DNA damage (Al Housseiny et al., 2020; De Grove et al., 2018; Ma 2020). Thus, we examined the expression of proinflammatory markers known to be expressed by lung epithelial cells. BEAS-2B cells exposed to uncoated SP did not exhibit significant inflammatory response (Al Housseiny et al., 2020), although, according to the RNA-seq analysis, the SP may induce gene expression related to an inflammatory response, as also indicated by other studies (Niranjan and Thakur 2017). It was suggested that the functional groups on the particle surface are sufficient to induce inflammatory response (Al Housseiny et al., 2020; De Grove et al., 2018; Totlandsdal et al., 2015) as well as a specific component of PM (Totlandsdal et al., 2015; Tuet et al., 2017a). For example, it was demonstrated that organic compounds in particles emitted from diesel engine exhaust (DEPs) were the main drivers for releasing epithelial IL-1β, IL-6, IL-8 and GM-CSF cytokines (De Grove et al., 2018; Totlandsdal et al., 2015). Furthermore, SP with varying surface composition induced the expression of proinflammatory genes compared to unmodified soot (Al Housseiny et al., 2020). This notion is also supported by this study, in which $SOA_{Nap}$-SP, induced a profound inflammatory response, whereas exposure to the SP, without significant particle surface functionalization or organic coating, induced only very minor inflammatory response.

Aromatic compounds such as PAHs are AhR ligands. It was shown that AhR induces the production of inflammatory cytokines and alters T cell differentiation (O'Driscoll and Mezrich 2018; Vogel et al., 2020). It was recently reported that environmentally persistent free radicals formed in combustion processes may activate AhR and induce Th17-related cytokines (IL-1β, IL-22, IL-33, keratinocyte-derived chemokine), leading to Th17 polarization and IL-17-dependent pulmonary inflammation (Jaligama et al., 2018), suggesting a direct link between the activation of AhR and inflammatory responses (O'Driscoll and Mezrich 2018; Vogel et al., 2020). Our RNA-seq results showed a profound IL-17 response, especially after exposure to $SOA_{Nap}$-SP. This result is in line with the involvement of PAH in AhR activation that mediates the inflammatory response. As shown by 2-D gas chromatography mass spectrometry (GC MS) and the aromaticity index from FT-ICR analysis, $SOA_{Nap}$-SP contained a high aromatic content, while $SOA_{\beta Pin}$-SP did not contain such moieties.

The acute response to inhaled particles is mainly coordinated by type 1 immune cells and cytokines, such as IFN-γ, IL-2, IL-12, IL-1β, IL-18 and TNF-α (Ma 2020; Totlandsdal et al., 2015; Tuet et al., 2017a). In our study, exposure to $SOA_{Nap}$-SP increased INF-γ, IL-12, IL-1β, and TNF-α compared to that of SP and $SOA_{\beta Pin}$-SP, suggesting that the early acute inflammatory response to SOA is involved with type 1 inflammation. Nevertheless, although immune cells were not directly tested in the study, genes involved in the immune response were differentially expressed after exposure to SP and SOA-SP in BEAS-2B cells. Among these DE genes are changes in plasminogen activator inhibitor-2 (SERPINB2), which serves as a marker of type 2 inflammation (T-helper type 2, Th2) and is considered the main mechanism of asthma (Singhania et al., 2018; Zhang et al., 2019). This suggests that both types of inflammatory responses are involved in SOA-induced inflammation. SERPINB2 is also considered to be regulated by AhR (Brauze et al., 2019; Zhang et al., 2019); it was shown that benzo[a]pyrene (BaP), a PAH used as a benchmark for carcinogenicity, induced SERPINB2 gene expression in the UT-SCC-34 laryngeal squamous cell carcinoma cell line, which was partially dependent on AhR (Brauze et al., 2019). However, in our study the levels of the SERPINB2 gene were equally upregulated for SP, $SOA_{\beta Pin}$-SP and $SOA_{Nap}$-SP, supporting an independent mechanism of SERPINB2 activation and AhR.

A crucial connection between cytokine production and ROS formation was previously found, as PM-induced cytokines such as IL-1α, IL-1β, IL-6, IL-8 and GM-CSF that were significantly decreased after treatment with radical scavengers/antioxidants (De Grove et al., 2018; Wang et al., 2017). The interplay between oxidative stress and inflammation can be activated by the signal transducer and activator of transcription 3 (STAT3) and MAPK, which were also expressed in this study and mediate the expression of a variety of genes in response to cellular stimuli (Ahmed et al., 2019; Kagan et al., 2017; Wang et al., 2017; Zheng et al., 2017).

### 4.3. Oxidative damage after exposure to SOA

PM toxicity has been associated with the chemical composition of the particles and with the ability of PM to generate ROS (Chowdhury et al., 2019; Tong et al., 2018; Verma et al., 2015). In this study, exposure to $SOA_{Nap}$-SP led to augmented peroxide levels and a higher abundance of lipid peroxidation products than that of $SOA_{\beta Pin}$-SP exposure (Offer et al., 2022). In addition, $SOA_{Nap}$-SP induced a higher ROS production and oxidative potential than that of $SOA_{\beta Pin}$-SP, as measured by OPROSI (Zhang et al., 2022). ROS yields (e.g. radicals, $H_2O_2$) and the oxidative potential of isoprene, β-pinene, and naphthalene-derived SOA, measured in water and surrogate lung fluid increased (Tong et al., 2018). In particular, naphthalene-derived SOA was found to release substantial amounts of $O_2\bullet-$ and $H_2O_2$. It is known that excess amounts of ROS can cause oxidative stress and contribute to the imbalance between ROS production and their elimination through protective mechanisms by antioxidants inducing a broad range of toxicological effects such as inflammation, mutations, and lipid and DNA damage (Ahmed et al., 2019; Alves and Pio 2005; Chowdhury et al., 2019; Chowdhury et al., 2018; Eaves et al., 2020; Han et al., 2020; Ito et al., 2019; Lima de Albuquerque et al., 2021; Tuet et al., 2017a). RNA-seq analysis showed a profound reduction in alcohol dehydrogenase (ADH), especially for

$SOA_{Nap}$-SP. Reduced ADH activity leads to a low concentration of reduced glutathione (GSH), prompting oxidative stress and carcinogenesis in lung cancer cells (Orywal et al., 2020). This supports the conclusion that exposure to $SOA_{Nap}$-SP induces an oxidative stress response with increased ROS and MDA levels and reduced ADH.

The DNA damage response was also remarkably higher for $SOA_{Nap}$-SP than for $SOA_{\beta Pin}$-SP, SP and CA. It was previously shown that naphthalene metabolites, metabolites 1,2-hydroxynaphthalene (NQH2), 1,4-NQH2, 1,2-naphthoquinone (1,2-NQ), and 1,4-NQ induced DNA damage in the presence of nicotinamide adenine dinucleotide (NADH) and metal ions (Ohnishi et al., 2018). However, in a study that evaluated the source contribution of various atmospheric organic aerosols, naphthalene-derived SOA was evaluated as one of the most important sources of atmospheric organic aerosol toxicity, and the results showed increased oxidative and inflammatory responses but minor effects on DNA damage (Fushimi et al., 2021). Our results suggest that due to the high ROS levels, oxidative stress and oxidative damage play a vital role in SOA toxicity, particularly for $SOA_{Nap}$-SP.

While this study provides novel information regarding the cellular response to β-pinene and naphthalene-derived SOA, it is not without limitations. β-pinene and naphthalene were used as representative (model) SOA precursors from biogenic and anthropogenic sources. However, these two precursors do not provide sharp discrimination by the apparent aliphatic and aromatic carbon backbone of the SOA precursors, which were partly maintained after aging. For example, aromatic compounds, such as p-cymene, may be released from vegetation and monoterpenes may be released from industrial processes or wood combustion for residential heating. Additionally, variations within the groups of biogenic and anthropogenic emissions may lead to the formation of different SOA. Consequently, several individual primary aerosols must be investigated under a broad range of relevant atmospheric conditions to connect physical and chemical aerosol properties to toxicological responses. Epithelial responses can be different when sample collection is performed over different time periods or locations. Furthermore, epithelial cytokine expression can be influenced by the particle size, as well as the experimental setup, the selected PM dose and epithelial cell culture. Finally, as RNA-Seq and pathway enrichment analysis have enabled the identification of pathways at the transcript level, more functional validation such as protein levels changes, will be necessary to demonstrate the effects on the phenotypes.

## 5. Conclusions

In the present study, human bronchial epithelial cells (BEAS-2B) were exposed to low levels of fresh SP coated by SOA from biogenic and anthropogenic SOA precursors ($SOA_{\beta Pin}$-SP and $SOA_{Nap}$-SP, respectively). The results highlight that substantially lower cytotoxic effects were observed with pure SP than SP coated with SOA. The differences in the chemical characteristics of the two SOAs studied led to different and varied cytotoxic responses. Transcriptomic gene analysis followed by pathway enrichment analysis revealed that major biological pathways influenced by SOA-SP are associated with elevated oxidative stress, inflammation and cytokine signaling, as well as dysregulated metabolic activities, that play crucial roles in airway toxicity. The induction of Nrf2 pathway has been found to be unique for SOA-SP compared to soot coated particles. Furthermore, the involvement of MMP in SOA toxicity is reported here for the first time, providing evidence of an intricate toxicological response to SOA exposure. In addition, anthropogenically derived SOAs can activate different pathways and have higher toxicological potency than that of biogenically derived SOAs, as naphthalene-derived SOAs induced stronger oxidative stress and genotoxic and inflammatory responses than those of β-pinene-derived SOA. Based on the comprehensive aerosol particle analysis we attribute this difference to the chemical composition, in which the aromatic compounds and higher oxidation state of the naphthalene-derived SOA lead to higher cytotoxic potential than that of SOA from β-pinene.

This study has profound environmental significance, as anthropogenic SOAs represent a substantial fraction of the PM mass in populated areas around the world and contribute to poor air quality. The high concentrations of anthropogenic SOAs in cities, which mainly originate from burning for residential use, industrial use and tailpipe emissions, lead to high concentrations of toxic aerosols in and downwind urban centers (Daellenbach et al., 2020; Fushimi et al., 2021; Lim et al., 2019). It is estimated that exposure to outdoor $PM_{2.5}$ has led to>8 million premature deaths (Burnett et al., 2018; Forouzanfar et al., 2016). This estimation is supported by recent global simulations that attribute 340,000 $PM_{2.5}$-related premature deaths per year to anthropogenic SOAs annually. However, large uncertainties regarding anthropogenic SOA sources still exist (Nault et al., 2021). Our study suggests that SOA is generally toxic even at low exposure doses, and anthropogenic SOA is more toxic than biogenic SOA based on structural differences in the most relevant SOA precursors. This means that anthropogenic SOA sources need to be better constrained, and their emissions and related SOAs need to be monitored and reduced.

Future work will be necessary to elucidate the atmospheric complexity of SOAs, and discover dynamic biological responses as a result of atmospheric aging. To fully assess the environmental health impacts of anthropogenic and biogenically derived SOA, a comprehensive protein analysis and additional biological functions in primary epithelial cells as well as coculture or 3D model systems would be of great interest.

## CRediT authorship contribution statement

**Michal Pardo:** Conceptualization, Investigation, Validation, Visualization. **Svenja Offer:** Investigation, Validation. **Elena Hartner:** Investigation, Validation. **Sebastiano Di Bucchianico:** Conceptualization, Investigation, Validation, Visualization, Writing – review & editing. **Christoph Bisig:** Investigation, Validation. **Stefanie Bauer:** Investigation, Validation. **Jana Pantzke:** Investigation, Validation. **Elias J. Zimmermann:** Investigation, Validation. **Xin Cao:** Investigation, Validation. **Stephanie Binder:** Investigation, Validation. **Evelyn Kuhn:** Investigation, Validation. **Anja Huber:** Investigation, Validation. **Seongho Jeong:** Investigation, Validation. **Uwe Käfer:** Investigation, Validation. **Eric Schneider:** Investigation, Validation. **Arunas Mesceriakovas:** Investigation, Validation. **Jan Bendl:** Investigation, Validation. **Ramona Brejcha:** Investigation, Validation. **Angela Buchholz:** Investigation, Validation. **Daniela Gat:** Investigation, Validation. **Thorsten Hohaus:** Conceptualization, Investigation, Validation. **Narges Rastak:** Formal analysis. **Erwin Karg:** Formal analysis. **Gert Jakobi:** Methodology, Validation. **Markus Kalberer:** Conceptualization, Supervision. **Tamara Kanashova:** Methodology, Validation. **Yue Hu:** Software. **Christoph Ogris:** Software. **Annalisa Marsico:** Conceptualization, Supervision. **Fabian Theis:** Conceptualization, Supervision. **Tali Shalit:** Software, Formal analysis. **Thomas Gröger:** Methodology, Validation. **Christopher P. Rüger:** Methodology, Validation. **Sebastian Oeder:** Methodology, Validation. **Jürgen Orasche:** Methodology, Validation. **Andreas Paul:** Methodology, Validation. **Till Ziehm:** Methodology, Validation. **Zhi-Hui Zhang:** Methodology, Validation. **Thomas Adam:** Conceptualization, Supervision. **Olli Sippula:** Conceptualization, Supervision. **Martin Sklorz:** Methodology, Validation. **Jürgen Schnelle-Kreis:** Methodology, Validation. **Hendryk Czech:** Conceptualization, Investigation, Formal analysis, Visualization. **Astrid Kiendler-Scharr:** Conceptualization, Supervision. **Ralf Zimmermann:** Conceptualization, Supervision. **Yinon Rudich:** Conceptualization, Supervision.

## Declaration of Competing Interest

The authors declare that they have no known competing financial interests or personal relationships that could have appeared to influence the work reported in this paper.

## Acknowledgements

We thank the Helmholtz International Laboratory aeroHEALTH (InterLabs-0005; www.aerohealth.eu) for granting this project. Y.R. acknowledges support from the Anita James Rosen Foundation. We thank William H. Brune (Pennsylvania State University) for providing the PAM reactor in conjunction with a PO for a PAM in this study, which was funded by the University of Rostock. Funding by the Horizon 2020 program for the EU FT-ICR MS project (European Network of Fourier-transform Ion Cyclotron-Resonance Mass Spectrometry Centers, Grant agreement ID: 731077) is gratefully acknowledged.

## Appendix A. Supplementary material

Additional experimental details, and methods including experimental set up and results. Supplementary data to this article can be found online at https://doi.org/10.1016/j.envint.2022.107366.

## References

Ahmed, C.M.S., Cui, Y., Frie, A.L., Burr, A., Kamath, R., Chen, J.Y., Rahman, A., Nordgren, T.M., Lin, Y.H., Bahreini, R., 2019. Exposure to Dimethyl Selenide (DMSe)-Derived Secondary Organic Aerosol Alters Transcriptomic Profiles in Human Airway Epithelial Cells. Environ. Sci. Technol. 53, 14660–14669.

Al Housseiny, H., Singh, M., Emile, S., Nicoleau, M., Wal, R.L.V., Silveyra, P., 2020. Identification of Toxicity Parameters Associated with Combustion Produced Soot Surface Chemistry and Particle Structure by in Vitro Assays. Biomedicines 8.

Alves, C.A., Pio, C.A., 2005. Secondary organic compounds in atmospheric aerosols: speciation and formation mechanisms. J. Braz. Chem. Soc. 16, 1017–1029.

Arashiro, M., Lin, Y.H., Sexton, K.G., Zhang, Z., Jaspers, I., Fry, R.C., Vizuete, W.G., Gold, A., Surratt, J.D., 2016. In vitro exposure to isoprene-derived secondary organic aerosol by direct deposition and its effects on COX-2 and IL-8 gene expression. Atmos. Chem. Phys. 16, 14079–14090.

Bai, H., Wu, M., Zhang, H., Tang, G., 2017. Chronic polycyclic aromatic hydrocarbon exposure causes DNA damage and genomic instability in lung epithelial cells. Oncotarget 8, 79034–79045.

Barmet, P., Dommen, J., DeCarlo, P.F., Tritscher, T., Praplan, A.P., Platt, S.M., Prévôt, A. S.H., Donahue, N.M., Baltensperger, U., 2012. OH clock determination by proton transfer reaction mass spectrometry at an environmental chamber. Atmos. Meas. Tech. 5, 647–656.

Borbon, A., Gilman, J.B., Kuster, W.C., Grand, N., Chevaillier, S., Colomb, A., Dolgorouky, C., Gros, V., Lopez, M., Sarda-Esteve, R., Holloway, J., Stutz, J., Petetin, H., McKeen, S., Beekmann, M., Warneke, C., Parrish, D.D., de Gouw, J.A., 2013. Emission ratios of anthropogenic volatile organic compounds in northern mid-latitude megacities: Observations versus emission inventories in Los Angeles and Paris. J. Geophys. Res.: Atmos. 118, 2041–2057.

Brauer, M., Freedman, G., Frostad, J., van Donkelaar, A., Martin, R.V., Dentener, F., Dingenen, R.v., Estep, K., Amini, H., Apte, J.S., Balakrishnan, K., Barregard, L., Broday, D., Feigin, V., Ghosh, S., Hopke, P.K., Knibbs, L.D., Kokubo, Y., Liu, Y., Ma, S., Morawska, L., Sangrador, J.L.T., Shaddick, G., Anderson, H.R., Vos, T., Forouzanfar, M.H., Burnett, R.T., Cohen, A., 2016. Ambient Air Pollution Exposure Estimation for the Global Burden of Disease 2013. Environ. Sci. & Technol. 50:79-88.

Brauze, D., Kiwerska, K., Bednarek, K., Grenman, R., Janiszewska, J., Giefing, M., Jarmuz-Szymczak, M., 2019. Expression of Serpin Peptidase Inhibitor B2 (SERPINB2) is regulated by Aryl hydrocarbon receptor (AhR). Chem. Biol. Interact. 309, 108700.

Bruns, E.A., El Haddad, I., Keller, A., Klein, F., Kumar, N.K., Pieber, S.M., Corbin, J.C., Slowik, J.G., Brune, W.H., Baltensperger, U., Prévôt, A.S.H., 2015. Inter-comparison of laboratory smog chamber and flow reactor systems on organic aerosol yield and composition. Atmos. Meas. Tech. 8, 2315–2332.

Brzóska, K., Bartłomiejczyk, T., Sochanowicz, B., Cymerman, M., Grudny, J., Kołakowski, J., Kapka-Skrzypczak, L., Kruszewski, M., Sliwiński, P., Roszkowski-Śliż, K., 2014. Matrix metalloproteinase 3 polymorphisms as a potential marker of enhanced susceptibility to lung cancer in chronic obstructive pulmonary disease subjects. Ann. Agric. Environ. Med. 21, 546–551.

Burnett, R., Chen, H., Szyszkowicz, M., Fann, N., Hubbell, B., Pope, C.A., Apte, J.S., Brauer, M., Cohen, A., Weichenthal, S., Coggins, J., Di, Q., Brunekreef, B., Frostad, J., Lim, S.S., Kan, H., Walker, K.D., Thurston, G.D., Hayes, R.B., Lim, C.C., Turner, M. C., Jerrett, M., Krewski, D., Gapstur, S.M., Diver, W.R., Ostro, B., Goldberg, D., Crouse, D.L., Martin, R.V., Peters, P., Pinault, L., Tjepkema, M., van Donkelaar, A., Villeneuve, P.J., Miller, A.B., Yin, P., Zhou, M., Wang, L., Janssen, N.A.H., Marra, M., Atkinson, R.W., Tsang, H., Quoc Thach, T., Cannon, J.B., Allen, R.T., Hart, J.E., Laden, F., Cesaroni, G., Forastiere, F., Weinmayr, G., Jaensch, A., Nagel, G., Concin, H., Spadaro, J.V., 2018. Global estimates of mortality associated with long-term exposure to outdoor fine particulate matter. Proc. Natl. Acad. Sci. 115:9592-9597.

Campen, M.J., Lund, A.K., Doyle-Eisele, M.L., McDonald, J.D., Knuckles, T.L., Rohr, A.C., Knipping, E.M., Mauderly, J.L., 2010. A comparison of vascular effects from complex and individual air pollutants indicates a role for monoxide gases and volatile hydrocarbons. Environ. Health Perspect. 118, 921–927.

Chowdhury, P.H., He, Q., Carmieli, R., Li, C., Rudich, Y., Pardo, M., 2019. Connecting the Oxidative Potential of Secondary Organic Aerosols with Reactive Oxygen Species in Exposed Lung Cells. Environ. Sci. Technol. 53, 13949–13958.

Chowdhury, P.H., He, Q., Lasitza Male, T., Brune, W.H., Rudich, Y., Pardo, M., 2018. Exposure of Lung Epithelial Cells to Photochemically Aged Secondary Organic Aerosol Shows Increased Toxic Effects. Environ. Sci. Technol. Lett. 5, 424–430.

Claeys, M., Iinuma, Y., Szmigielski, R., Surratt, J.D., Blockhuys, F., Van Alsenoy, C., Böge, O., Sierau, B., Gómez-González, Y., Vermeylen, R., Van der Veken, P., Shahgholi, M., Chan, A.W.H., Herrmann, H., Seinfeld, J.H., Maenhaut, W., 2009. Terpenylic Acid and Related Compounds from the Oxidation of α-Pinene: Implications for New Particle Formation and Growth above Forests. Environ. Sci. Technol. 43, 6976–6982.

Claflin, M.S., Ziemann, P.J., 2019. Thermal desorption behavior of hemiacetal, acetal, ether, and ester oligomers. Aerosol Sci. Technol. 53, 473–484.

Cohen, A.J., Brauer, M., Burnett, R., Anderson, H.R., Frostad, J., Estep, K., Balakrishnan, K., Brunekreef, B., Dandona, L., Dandona, R., Feigin, V., Freedman, G., Hubbell, B., Jobling, A., Kan, H., Knibbs, L., Liu, Y., Martin, R., Morawska, L., Pope, C.A., 3rd; Shin, H., Straif, K., Shaddick, G., Thomas, M., van Dingenen, R., van Donkelaar, A., Vos, T., Murray, C.J.L., 2017. Forouzanfar, M.H. Estimates and 25-year trends of the global burden of disease attributable to ambient air pollution: an analysis of data from the Global Burden of Diseases Study 2015. Lancet 389:1907-1918.

Cui, N., Hu, M., Khalil, R.A., 2017. Biochemical and Biological Attributes of Matrix Metalloproteinases. Prog. Mol. Biol. Transl. Sci. 147, 1–73.

Daellenbach, K.R., Uzu, G., Jiang, J., Cassagnes, L.-E., Leni, Z., Vlachou, A., Stefenelli, G., Canonaco, F., Weber, S., Segers, A., Kuenen, J.J.P., Schaap, M., Favez, O., Albinet, A., Aksoyoglu, S., Dommen, J., Baltensperger, U., Geiser, M., El Haddad, I., Jaffrezo, J.-L., Prévôt, A.S.H., 2020. Sources of particulate-matter air pollution and its oxidative potential in Europe. Nature 587, 414–419.

Dagouassat, M., Lanone, S., Boczkowski, J., 2012. Interaction of matrix metalloproteinases with pulmonary pollutants. Eur. Respir. J. 39, 1021–1032.

Das, A., Habib, G., Vivekanandan, P., Kumar, A., 2021. Reactive oxygen species production and inflammatory effects of ambient PM2.5 -associated metals on human lung epithelial A549 cells “one year-long study”: The Delhi chapter. Chemosphere 262:128305.

De Grove, K.C., Provoost, S., Brusselle, G.G., Joos, G.F., Maes, T., 2018. Insights in particulate matter-induced allergic airway inflammation: Focus on the epithelium. Clin. Exp. Allergy 48, 773–786.

Di Bucchianico, S., Cappellini, F., Le Bihanic, F., Zhang, Y., Dreij, K., Karlsson, H.L., 2017. Genotoxicity of TiO2 nanoparticles assessed by mini-gel comet assay and micronucleus scoring with flow cytometry. Mutagenesis 32, 127–137.

Eaves, L.A., Smeester, L., Hartwell, H.J., Lin, Y.-H., Arashiro, M., Zhang, Z., Gold, A., Surratt, J.D., Fry, R.C., 2020. Isoprene-Derived Secondary Organic Aerosol Induces the Expression of MicroRNAs Associated with Inflammatory/Oxidative Stress Response in Lung Cells. Chem. Res. Toxicol. 33, 381–387.

Forouzanfar, M.H., Afshin, A., Alexander, L.T., Anderson, H.R., Bhutta, Z.A., Biryukov, S., Brauer, M., Burnett, R., Cercy, K., Charlson, F.J., Cohen, A.J., Dandona, L., Estep, K., Ferrari, A.J., Frostad, J.J., Fullman, N., Gething, P.W., Godwin, W.W., Griswold, M., Hay, S.I., Kinfu, Y., Kyu, H.H., Larson, H.J., Liang, X., Lim, S.S., Liu, P.Y., Lopez, A.D., Lozano, R., Marczak, L., Mensah, G.A., Mokdad, A.H., Moradi-Lakeh, M., Naghavi, M., Neal, B., Reitsma, M.B., Roth, G.A., Salomon, J.A., Sur, P.J., Vos, T., Wagner, J.A., Wang, H., Zhao, Y., Zhou, M., Aasvang, G.M., Abajobir, A.A., Abate, K. H., Abbafati, C., Abbas, K.M., Abd-Allah, F., Abdulle, A.M., Abera, S.F., Abraham, B., Abu-Raddad, L.J., Abyu, G.Y., Adebiyi, A.O., Adedeji, I.A., Ademi, Z., Adou, A.K., Adsuar, J.C., Agardh, E.E., Agarwal, A., Agrawal, A., Kiadaliri, A.A., Ajala, O.N., Akinyemiju, T.F., Al-Aly, Z., Alam, K., Alam, N.K.M., Aldhahri, S.F., Aldridge, R.W., Alemu, Z.A., Ali, R., Alkerwi, A.a., Alla, F., Allebeck, P., Alsharif, U., Altirkawi, K.A., Martin, E.A., Alvis-Guzman, N., Amare, A.T., Amberbir, A., Amegah, A.K., Amini, H., Ammar, W., Amrock, S.M., Andersen, H.H., Anderson, B.O., Antonio, C.A.T., Anwari, P., Ärnlöv, J., Artaman, A., Asayesh, H., Asghar, R.J., Assadi, R., Atique, S., Avokpaho, E.F.G.A., Awasthi, A., Quintanilla, B.P.A., Azzopardi, P., Bacha, U., Badawi, A., Bahit, M.C., Balakrishnan, K., Barac, A., Barber, R.M., Barker-Collo, S.L., Bärnighausen, T., Barquera, S., Barregard, L., Barrero, L.H., Basu, S., Batis, C., Bazargan-Hejazi, S., Beardsley, J., Bedi, N., Beghi, E., Bell, B., Bell, M.L., Bello, A.K., Bennett, D.A., Bensenor, I.M., Berhane, A., Bernabé, E., Betsu, B.D., Beyene, A.S., Bhala, N., Bhansali, A., Bhatt, S., Biadgilign, S., Bikbov, B., Bisanzio, D., Bjertness, E., Blore, J.D., Borschmann, R., Boufous, S., Bourne, R.R.A., Brainin, M., Brazinova, A., Breitborde, N.J.K., Brenner, H., Broday, D.M., Brugha, T.S., Brunekreef, B., Butt, Z. A., Cahill, L.E., Calabria, B., Campos-Nonato, I.R., Cárdenas, R., Carpenter, D.O., Carrero, J.J., Casey, D.C., Castañeda-Orjuela, C.A., Rivas, J.C., Castro, R.E., Catalá-López, F., Chang, J.-C., Chiang, P.P.-C., Chibalabala, M., Chimed-Ochir, O., Chisumpa, V.H., Chitheer, A.A., Choi, J.-Y.J., Christensen, H., Christopher, D.J., Ciobanu, L.G., Coates, M.M., Colquhoun, S.M., Manzano, A.G.C., Cooper, L.T., Cooperrider, K., Cornaby, L., Cortinovis, M., Crump, J.A., Cuevas-Nasu, L., Damasceno, A., Dandona, R., Darby, S.C., Dargan, P.I., das Neves, J., Davis, A.C., Davletov, K., de Castro, E.F., De la Cruz-Góngora, V., De Leo, D., Degenhardt, L., Del Gobbo, L.C., del Pozo-Cruz, B., Dellavalle, R.P., Deribew, A., Jarlais, D.C.D., Dharmaratne, S.D., Dhillon, P.K., Diaz-Torné, C., Dicker, D., Ding, E.L., Dorsey, E.R., Doyle, K.E., Driscoll, T.R., Duan, L., Dubey, M., Duncan, B.B., Elyazar, I., Endries, A. Y., Ermakov, S.P., Erskine, H.E., Eshrati, B., Esteghamati, A., Fahimi, S., Faraon, E.J. A., Farid, T.A., Farinha, C.S.e.S., Faro, A., Farvid, M.S., Farzadfar, F., Feigin, V.L., Fereshtehnejad, S.-M., Fernandes, J.G., Fischer, F., Fitchett, J.R.A., Fleming, T., Foigt, N., Foreman, K., Fowkes, F.G.R., Franklin, R.C., Fürst, T., Futran, N.D., Gakidou, E., Garcia-Basteiro, A.L., Gebrehiwot, T.T., Gebremedhin, A.T., Geleijnse, J.M., Gessner, B.D., Giref, A.Z., Giroud, M., Gishu, M.D., Giussani, G., Goenka, S., Gomez-Cabrera, M.C., Gomez-Dantes, H., Gona, P., Goodridge, A., Gopalani, S.V., Gotay, C.C., Goto, A., Gouda, H.N., Gugnani, H.C., Guillemin, F., Guo, Y., Gupta, R.,

Gupta, R., Gutiérrez, R.A., Haagsma, J.A., Hafezi-Nejad, N., Haile, D., Hailu, G.B., Halasa, Y.A., Hamadeh, R.R., Hamidi, S., Handal, A.J., Hankey, G.J., Hao, Y., Harb, H.L., Harikrishnan, S., Haro, J.M., Hassanvand, M.S., Hassen, T.A., Havmoeller, R., Heredia-Pi, I.B., Hernández-Llanes, N.F., Heydarpour, P., Hoek, H.W., Hoffman, H.J., Horino, M., Horita, N., Hosgood, H.D., Hoy, D.G., Hsairi, M., Htet, A.S., Hu, G., Huang, J.J., Husseini, A., Hutchings, S.J., Huybrechts, I., Iburg, K.M., Idrisov, B.T., Ileanu, B.V., Inoue, M., Jacobs, T.A., Jacobsen, K.H., Jahanmehr, N., Jakovljevic, M. B., Jansen, H.A.F.M., Jassal, S.K., Javanbakht, M., Jayaraman, S.P., Jayatilleke, A.U., Jee, S.H., Jeemon, P., Jha, V., Jiang, Y., Jibat, T., Jin, Y., Johnson, C.O., Jonas, J.B., Kabir, Z., Kalkonde, Y., Kamal, R., Kan, H., Karch, A., Karema, C.K., Karimkhani, C., Kasaeian, A., Kaul, A., Kawakami, N., Kazi, D.S., Keiyoro, P.N., Kemmer, L., Kemp, A. H., Kengne, A.P., Keren, A., Kesavachandran, C.N., Khader, Y.S., Khan, A.R., Khan, E. A., Khan, G., Khang, Y.-H., Khatibzadeh, S., Khera, S., Khoja, T.A.M., Khubchandani, J., Kieling, C., Kim, C.-i., Kim, D., Kimokoti, R.W., Kissoon, N., Kivipelto, M., Knibbs, L.D., Kokubo, Y., Kopec, J.A., Koul, P.A., Koyanagi, A., Kravchenko, M., Kromhout, H., Krueger, H., Ku, T., Defo, B.K., Kuchenbecker, R.S., Bicer, B.K., Kuipers, E.J., Kumar, G.A., Kwan, G.F., Lal, D.K., Lalloo, R., Lallukka, T., Lan, Q., Larsson, A., Latif, A.A., Lawrynowicz, A.E.B., Leasher, J.L., Leigh, J., Leung, J., Levi, M., Li, X., Li, Y., Liang, J., Liu, S., Lloyd, B.K., Logroscino, G., Lotufo, P.A., Lunevicius, R., MacIntyre, M., Mahdavi, M., Majdan, M., Majeed, A., Malekzadeh, R., Malta, D.C., Manamo, W. A.A., Mapoma, C.C., Marcenes, W., Martin, R.V., Martinez-Raga, J., Masiye, F., Matsushita, K., Matzopoulos, R., Mayosi, B.M., McGrath, J.J., McKee, M., Meaney, P. A., Medina, C., Mehari, A., Mejia-Rodriguez, F., Mekonnen, A.B., Melaku, Y.A., Memish, Z.A., Mendoza, W., Mensink, G.B.M., Meretoja, A., Meretoja, T.J., Mesfin, Y.M., Mhimbira, F.A., Millear, A., Miller, T.R., Mills, E.J., Mirarefin, M., Misganaw, A., Mock, C.N., Mohammadi, A., Mohammed, S., Mola, G.L.D., Monasta, L., Hernandez, J.C.M., Montico, M., Morawska, L., Mori, R., Mozaffarian, D., Mueller, U. O., Mullany, E., Mumford, J.E., Murthy, G.V.S., Nachega, J.B., Naheed, A., Nangia, V., Nassiri, N., Newton, J.N., Ng, M., Nguyen, Q.L., Nisar, M.I., Pete, P.M.N., Norheim, O.F., Norman, R.E., Norrving, B., Nyakarahuka, L., Obermeyer, C.M., Ogbo, F.A., Oh, I.-H., Oladimeji, O., Olivares, P.R., Olsen, H., Olusanya, B.O., Olusanya, J.O., Opio, J.N., Oren, E., Orozco, R., Ortiz, A., Ota, E., Pa, M., Pana, A., Park, E.-K., Parry, C.D., Parsaeian, M., Patel, T., Caicedo, A.J.P., Patil, S.T., Patten, S. B., Patton, G.C., Pearce, N., Pereira, D.M., Perico, N., Pesudovs, K., Petzold, M., Phillips, M.R., Piel, F.B., Pillay, J.D., Plass, D., Polinder, S., Pond, C.D., Pope, C.A., Pope, D., Popova, S., Poulton, R.G., Pourmalek, F., Prasad, N.M., Qorbani, M., Rabiee, R.H.S., Radfar, A., Rafay, A., Rahimi-Movaghar, V., Rahman, M., Rahman, M.H.U., Rahman, S.U., Rai, R.K., Rajsic, S., Raju, M., Ram, U., Rana, S.M., Ranganathan, K., Rao, P., García, C.A.R., Refaat, A.H., Rehm, C.D., Rehm, J., Reinig, N., Remuzzi, G., Resnikoff, S., Ribeiro, A.L., Rivera, J.A., Roba, H.S., Rodriguez, A., Rodriguez-Ramirez, S., Rojas-Rueda, D., Roman, Y., Ronfani, L., Roshandel, G., Rothenbacher, D., Roy, A., Saleh, M.M., Sanabria, J.R., Sanchez-Riera, L., Sanchez-Niño, M.D., Sánchez-Pimienta, T.G., Sandar, L., Santomauro, D.F., Santos, I.S., Sarmiento-Suarez, R., Sartorius, B., Satpathy, M., Savic, M., Sawhney, M., Schmidhuber, J., Schmidt, M.I., Schneider, I.J.C., Schöttker, B., Schutte, A.E., Schwebel, D.C., Scott, J.G., Seedat, S., Sepanlou, S.G., Servan-Mori, E.E., Shaddick, G., Shaheen, A., Shahraz, S., Shaikh, M.A., Levy, T.S., Sharma, R., She, J., Sheikhbahaei, S., Shen, J., Sheth, K.N., Shi, P., Shibuya, K., Shigematsu, M., Shin, M.-J., Shiri, R., Shishani, K., Shiue, I., Shrime, M.G., Sigfusdottir, I.D., Silva, D.A.S., Silveira, D.G.A., Silverberg, J.I., Simard, E.P., Sindi, S., Singh, A., Singh, J.A., Singh, P.K., Slepak, E.L., Soljak, M., Soneji, S., Sorensen, R.J.D., Sposato, L.A., Sreeramareddy, C.T., Stathopoulou, V., Steckling, N., Steel, N., Stein, D.J., Stein, M. B., Stöckl, H., Stranges, S., Stroumpoulis, K., Sunguya, B.F., Swaminathan, S., Sykes, B.L., Szoeke, C.E.I., Tabarés-Seisdedos, R., Takahashi, K., Talongwa, R.T., Tandon, N., Tanne, D., Tavakkoli, M., Taye, B.W., Taylor, H.R., Tedla, B.A., Tefera, W.M., Tegegne, T.K., Tekle, D.Y., Terkawi, A.S., Thakur, J.S., Thomas, B.A., Thomas, M.L., Thomson, A.J., Thorne-Lyman, A.L., Thrift, A.G., Thurston, G.D., Tillmann, T., Tobe-Gai, R., Tobollik, M., Topor-Madry, R., Topouzis, F., Towbin, J.A., Tran, B.X., Dimbuene, Z.T., Tsilimparis, N., Tura, A.K., Tuzcu, E.M., Tyrovolas, S., Ukwaja, K.N., Undurraga, E.A., Uneke, C.J., Uthman, O.A., van Donkelaar, A., van Os, J., Varakin, Y.Y., Vasankari, T., Veerman, J.L., Venketasubramanian, N., Violante, F.S., Vollset, S.E., Wagner, G.R., Waller, S.G., Wang, J.L., Wang, L., Wang, Y., Weichenthal, S., Weiderpass, E., Weintraub, R.G., Werdecker, A., Westerman, R., Whiteford, H.A., Wijeratne, T., Wiysonge, C.S., Wolfe, C.D.A., Won, S., Woolf, A.D., Wubshet, M., Xavier, D., Xu, G., Yadav, A.K., Yakob, B., Yalew, A.Z., Yano, Y., Yaseri, M., Ye, P., Yip, P., Yonemoto, N., Yoon, S.-J., Younis, M.Z., Yu, C., Zaidi, Z., Zaki, M.E.S., Zhu, J., Zipkin, B., Zodpey, S., Zuhlke, L.J., Murray, C.J.L., 2016. Global, regional, and national comparative risk assessment of 79 behavioural, environmental and occupational, and metabolic risks or clusters of risks, 1990–2015: a systematic analysis for the Global Burden of Disease Study 2015. The Lancet 388:1659-1724.

Fushimi, A., Nakajima, D., Furuyama, A., Suzuki, G., Ito, T., Sato, K., Fujitani, Y., Kondo, Y., Yoshino, A., Ramasamy, S., Schauer, J.J., Fu, P., Takahashi, Y., Saitoh, K., Saito, S., Takami, A., 2021. Source contributions to multiple toxic potentials of atmospheric organic aerosols. Sci. Total Environ. 773, 145614.

Gu, S., Guenther, A., Faiola, C., 2021. Effects of Anthropogenic and Biogenic Volatile Organic Compounds on Los Angeles Air Quality. Environ. Sci. Technol. 55, 12191–12201.

Guenther, A., Hewitt, C.N., Erickson, D., Fall, R., Geron, C., Graedel, T., Harley, P., Klinger, L., Lerdau, M., Mckay, W.A., Pierce, T., Scholes, B., Steinbrecher, R., Tallamraju, R., Taylor, J., Zimmerman, P., 1995. A global model of natural volatile organic compound emissions. J. Geophys. Res.: Atmos. 100, 8873–8892.

Han, J., Wang, S., Yeung, K., Yang, D., Gu, W., Ma, Z., Sun, J., Wang, X., Chow, C.W., Chan, A.W.H., Peng, H., 2020. Proteome-wide effects of naphthalene-derived secondary organic aerosol in BEAS-2B cells are caused by short-lived unsaturated carbonyls. Proc. Natl. Acad. Sci. U. S. A. 117, 25386–25395.

Han, Y., Gao, S., Muegge, K., Zhang, W., Zhou, B., 2015. Advanced Applications of RNA Sequencing and Challenges. Bioinf. Biol. Insights 9, 29–46.

Ito, T., Bekki, K., Fujitani, Y., Hirano, S., 2019. The toxicological analysis of secondary organic aerosol in human lung epithelial cells and macrophages. Environ. Sci. Pollut. Res. 26, 22747–22755.

Jaligama, S., Patel, V.S., Wang, P., Sallam, A., Harding, J., Kelley, M., Mancuso, S.R., Dugas, T.R., Cormier, S.A., 2018. Radical containing combustion derived particulate matter enhance pulmonary Th17 inflammation via the aryl hydrocarbon receptor. Part. Fibre Toxicol. 15, 20.

Jia, C., Batterman, S., 2010. A critical review of naphthalene sources and exposures relevant to indoor and outdoor air. Int. J. Environ. Res. Public Health 7, 2903–2939.

Käfer, U., Gröger, T., Rüger, C.P., Czech, H., Saraji-Bozorgzad, M., Wilharm, T., Zimmermann, R., 2019. Direct inlet probe – High-resolution time-of-flight mass spectrometry as fast technique for the chemical description of complex high-boiling samples. Talanta 202, 308–316.

Kagan, P., Sultan, M., Tachlytski, I., Safran, M., Ben-Ari, Z., 2017. Both MAPK and STAT3 signal transduction pathways are necessary for IL-6-dependent hepatic stellate cells activation. PLoS ONE 12, e0176173.

Kalberer, M., Paulsen, D., Sax, M., Steinbacher, M., Dommen, J., Prevot, A.S., Fisseha, R., Weingartner, E., Frankevich, V., Zenobi, R., Baltensperger, U., 2004. Identification of polymers as major components of atmospheric organic aerosols. Science 303, 1659–1662.

Kang, E., Root, M.J., Toohey, D.W., Brune, W.H., 2007. Introducing the concept of Potential Aerosol Mass (PAM). Atmos. Chem. Phys. 7, 5727–5744.

Kenseth, C.M., Huang, Y., Zhao, R., Dalleska, N.F., Hethcox, J.C., Stoltz, B.M., Seinfeld, J. H., 2018. Synergistic O<sub>3</sub> + OH oxidation pathway to extremely low-volatility dimers revealed in β-pinene secondary organic aerosol. Proc. Natl. Acad. Sci. 115, 8301–8306.

Khan, F., Kwapiszewska, K., Zhang, Y., Chen, Y., Lambe, A.T., Kołodziejczyk, A., Jalal, N., Rudzinski, K., Martínez-Romero, A., Fry, R.C., Surratt, J.D., Szmigielski, R., 2021. Toxicological Responses of α-Pinene-Derived Secondary Organic Aerosol and Its Molecular Tracers in Human Lung Cell Lines. Chem. Res. Toxicol. 34, 817–832.

Koch, B.P., Dittmar, T., 2006. From mass to structure: an aromaticity index for high-resolution mass data of natural organic matter. Rapid Commun. Mass Spectrom. 20, 926–932.

Koch, C.M., Chiu, S.F., Akbarpour, M., Bharat, A., Ridge, K.M., Bartom, E.T., Winter, D. R., 2018. A Beginner's Guide to Analysis of RNA Sequencing Data. Am. J. Respir. Cell Mol. Biol. 59, 145–157.

Kolb, C.E., Worsnop, D.R., 2012. Chemistry and Composition of Atmospheric Aerosol Particles. Annu. Rev. Phys. Chem. 63, 471–491.

Kopaczyk, J.M., Warguła, J., Jelonek, T., 2020. The variability of terpenes in conifers under developmental and environmental stimuli. Environ. Exp. Bot. 180, 104197.

Kroll, J.H., Donahue, N.M., Jimenez, J.L., Kessler, S.H., Canagaratna, M.R., Wilson, K.R., Altieri, K.E., Mazzoleni, L.R., Wozniak, A.S., Bluhm, H., Mysak, E.R., Smith, J.D., Kolb, C.E., Worsnop, D.R., 2011. Carbon oxidation state as a metric for describing the chemistry of atmospheric organic aerosol. Nat. Chem. 3, 133–139.

Kroll, J.H., Seinfeld, J.H., 2008. Chemistry of secondary organic aerosol: Formation and evolution of low-volatility organics in the atmosphere. Atmos. Environ. 42, 3593–3624.

Kuo, C.S., Pavlidis, S., Zhu, J., Loza, M., Baribaud, F., Rowe, A., Pandis, I., Gibeon, D., Hoda, U., Sousa, A., Wilson, S.J., Howarth, P., Shaw, D., Fowler, S., Dahlen, B., Chanez, P., Krug, N., Sandstrom, T., Fleming, L., Corfield, J., Auffray, C., Djukanovic, R., Sterk, P.J., Guo, Y., Adcock, I.M., Chung, K.F., 2019. Contribution of airway eosinophils in airway wall remodeling in asthma: Role of MMP-10 and MET. Allergy 74, 1102–1112.

Lambe, A.T., Ahern, A.T., Williams, L.R., Slowik, J.G., Wong, J.P.S., Abbatt, J.P.D., Brune, W.H., Ng, N.L., Wright, J.P., Croasdale, D.R., Worsnop, D.R., Davidovits, P., Onasch, T.B., 2011. Characterization of aerosol photooxidation flow reactors: heterogeneous oxidation, secondary organic aerosol formation and cloud condensation nuclei activity measurements. Atmos. Meas. Tech. 4, 445–461.

Lim, C.Y., Hagan, D.H., Coggon, M.M., Koss, A.R., Sekimoto, K., de Gouw, J., Warneke, C., Cappa, C.D., Kroll, J.H., 2019. Secondary organic aerosol formation from the laboratory oxidation of biomass burning emissions. Atmos. Chem. Phys. 19, 12797–12809.

Lima de Albuquerque, Y., Berger, E., Tomaz, S., George, C., Géloën, A., 2021. Evaluation of the Toxicity on Lung Cells of By-Products Present in Naphthalene Secondary Organic Aerosols. Life 11:319.

Lin, Y.H., Arashiro, M., Clapp, P.W., Cui, T., Sexton, K.G., Vizuete, W., Gold, A., Jaspers, I., Fry, R.C., Surratt, J.D., 2017. Gene Expression Profiling in Human Lung Cells Exposed to Isoprene-Derived Secondary Organic Aerosol. Environ. Sci. Technol. 51, 8166–8175.

Longhin, E., Holme, J.A., Gualtieri, M., Camatini, M., Øvrevik, J., 2018. Milan winter fine particulate matter (wPM2.5) induces IL-6 and IL-8 synthesis in human bronchial BEAS-2B cells, but specifically impairs IL-8 release. Toxicol. In Vitro 52, 365–373.

Lund, A.K., Doyle-Eisele, M., Lin, Y.H., Arashiro, M., Surratt, J.D., Holmes, T., Schilling, K.A., Seinfeld, J.H., Rohr, A.C., Knipping, E.M., McDonald, J.D., 2013. The effects of α-pinene versus toluene-derived secondary organic aerosol exposure on the expression of markers associated with vascular disease. Inhal Toxicol. 25, 309–324.

Ma, Q., 2020. Polarization of Immune Cells in the Pathologic Response to Inhaled Particulates. Front. Immunol. 11.

Manisalidis, I., Stavropoulou, E., Stavropoulos, A., Bezirtzoglou, E., 2020. Environmental and Health Impacts of Air Pollution: A Review. Front. Public Health 8, 14.

Mehra, A., Krechmer, J.E., Lambe, A., Sarkar, C., Williams, L., Khalaj, F., Guenther, A., Jayne, J., Coe, H., Worsnop, D., Faiola, C., Canagaratna, M., 2020. Oligomer and highly oxygenated organic molecule formation from oxidation of oxygenated

monoterpenes emitted by California sage plants. Atmos. Chem. Phys. 20, 10953–10965.
Nault, B.A., Jo, D.S., McDonald, B.C., Campuzano-Jost, P., Day, D.A., Hu, W., Schroder, J.C., Allan, J., Blake, D.R., Canagaratna, M.R., Coe, H., Coggon, M.M., DeCarlo, P.F., Diskin, G.S., Dunmore, R., Flocke, F., Fried, A., Gilman, J.B., Gkatzelis, G., Hamilton, J.F., Hanisco, T.F., Hayes, P.L., Henze, D.K., Hodzic, A., Hopkins, J., Hu, M., Huey, L.G., Jobson, B.T., Kuster, W.C., Lewis, A., Li, M., Liao, J., Nawaz, M.O., Pollack, I.B., Peischl, J., Rappenglück, B., Reeves, C.E., Richter, D., Roberts, J.M., Ryerson, T.B., Shao, M., Sommers, J.M., Walega, J., Warneke, C., Weibring, P., Wolfe, G.M., Young, D.E., Yuan, B., Zhang, Q., de Gouw, J.A., Jimenez, J.L., 2021. Secondary organic aerosols from anthropogenic volatile organic compounds contribute substantially to air pollution mortality. Atmos. Chem. Phys. 21, 11201–11224.
Ng, N.L., Canagaratna, M.R., Jimenez, J.L., Chhabra, P.S., Seinfeld, J.H., Worsnop, D.R., 2011. Changes in organic aerosol composition with aging inferred from aerosol mass spectra. Atmos. Chem. Phys. 11, 6465–6474.
Niranjan, R., Thakur, A.K., 2017. The Toxicological Mechanisms of Environmental Soot (Black Carbon) and Carbon Black: Focus on Oxidative Stress and Inflammatory Pathways. Frontiers in immunology 8:763-763.
O'Driscoll, C.A., Mezrich, J.D., 2018. The Aryl Hydrocarbon Receptor as an Immune-Modulator of Atmospheric Particulate Matter-Mediated Autoimmunity. Front. Immunol. 9.
Offer, S., Hartner, E., Bucchianico, S.D., Bisig, C., Bauer, S., Pantzke, J., Zimmermann, E. J., Cao, X., Binder, S., Kuhn, E., Huber, A., Jeong, S., Käfer, U., Martens, P., Mesceriakovas, A., Bendl, J., Brejcha, R., Buchholz, A., Gat, D., Hohaus, T., Rastak, N., Jakobi, G., Kalberer, M., Kanashova, T., Hu, Y., Ogris, C., Marsico, A., Theis, F., Pardo, M., Gröger, T., Oeder, S., Orasche, J., Paul, A., Ziehm, T., Zhang, Z.-H., Adam, T., Sippula, O., Sklorz, M., Schnelle-Kreis, J., Czech, H., Kiendler-Scharr, A., Rudich, Y., Zimmermann, R., 2022. Effect of Atmospheric Aging on Soot Particle Toxicity in Lung Cell Models at the Air-Liquid Interface: Differential Toxicological Impacts of Biogenic and Anthropogenic Secondary Organic Aerosols (SOAs). Environ. Health Perspect. 130, 027003.
Ohnishi, S., Hiraku, Y., Hasegawa, K., Hirakawa, K., Oikawa, S., Murata, M., Kawanishi, S., 2018. Mechanism of oxidative DNA damage induced by metabolites of carcinogenic naphthalene. Mutation Research/Genetic Toxicology and Environmental Mutagenesis 827, 42–49.
Orywal, K., Jelski, W., KozŁowski, M.D., Mroczko, B., 2020. Activity of Alcohol Dehydrogenase and Aldehyde Dehydrogenase in Lung Cancer Cells. Anticancer Res. 40, 3857–3863.
Pardo, M., Katra, I., Schaeur, J.J., Rudich, Y., 2017. Mitochondria-mediated oxidative stress induced by desert dust in rat alveolar macrophages. Geohealth 1, 4–16.
Pardo, M., Qiu, X., Zimmermann, R., Rudich, Y., 2020. Particulate Matter Toxicity Is Nrf2 and Mitochondria Dependent: The Roles of Metals and Polycyclic Aromatic Hydrocarbons. Chem. Res. Toxicol. 33, 1110–1120.
Paur, H.-R., Cassee, F.R., Teeguarden, J., Fissan, H., Diabate, S., Aufderheide, M., Kreyling, W.G., Hänninen, O., Kasper, G., Riediker, M., Rothen-Rutishauser, B., Schmid, O., 2011. In-vitro cell exposure studies for the assessment of nanoparticle toxicity in the lung—A dialog between aerosol science and biology. J. Aerosol Sci. 42, 668–692.
Pöschl, U., Shiraiwa, M., 2015. Multiphase Chemistry at the Atmosphere-Biosphere Interface Influencing Climate and Public Health in the Anthropocene. Chem. Rev. 115, 4440–4475.
Schnitzler, E.G., Dutt, A., Charbonneau, A.M., Olfert, J.S., Jäger, W., 2014. Soot Aggregate Restructuring Due to Coatings of Secondary Organic Aerosol Derived from Aromatic Precursors. Environ. Sci. Technol. 48, 14309–14316.
Shi, Y., Zeng, Z., Liu, J., Pi, Z., Zou, P., Deng, Q., Ma, X., Qiao, F., Xiong, W., Zhou, C., Zeng, Q., Xiao, R., 2021. Particulate matter promotes hyperpigmentation via AhR/MAPK signaling activation and by increasing α-MSH paracrine levels in keratinocytes. Environ. Pollut. 278, 116850.
Singhania, A., Wallington, J.C., Smith, C.G., Horowitz, D., Staples, K.J., Howarth, P.H., Gadola, S.D., Djukanović, R., Woelk, C.H., Hinks, T.S.C., 2018. Multitissue Transcriptomics Delineates the Diversity of Airway T Cell Functions in Asthma. Am. J. Respir. Cell Mol. Biol. 58, 261–270.
Son, Y., Cheong, Y.-K., Kim, N.-H., Chung, H.-T., Kang, D.G., Pae, H.-O., 2011. Mitogen-Activated Protein Kinases and Reactive Oxygen Species: How Can ROS Activate MAPK Pathways? J. Signal Transduction 2011, 792639.
Tong, H., Lakey, P.S.J., Arangio, A.M., Socorro, J., Shen, F., Lucas, K., Brune, W.H., Pöschl, U., Shiraiwa, M., 2018. Reactive Oxygen Species Formed by Secondary Organic Aerosols in Water and Surrogate Lung Fluid. Environ. Sci. Technol. 52, 11642–11651.
Totlandsdal, A.I., Låg, M., Lilleaas, E., Cassee, F., Schwarze, P., 2015. Differential proinflammatory responses induced by diesel exhaust particles with contrasting PAH and metal content. Environ. Toxicol. 30, 188–196.
Tuet, W.Y., Chen, Y., Fok, S., Champion, J.A., Ng, N.L., 2017a. Inflammatory responses to secondary organic aerosols (SOA) generated from biogenic and anthropogenic precursors. Atmos. Chem. Phys. 17, 11423–11440.
Tuet, W.Y., Chen, Y., Fok, S., Gao, D., Weber, R.J., Champion, J.A., Ng, N.L., 2017b. Chemical and cellular oxidant production induced by naphthalene secondary organic aerosol (SOA): effect of redox-active metals and photochemical aging. Sci. Rep. 7, 15157.
Verma, V., Fang, T., Xu, L., Peltier, R.E., Russell, A.G., Ng, N.L., Weber, R.J., 2015. Organic Aerosols Associated with the Generation of Reactive Oxygen Species (ROS) by Water-Soluble PM2.5. Environ. Sci. Technol. 49, 4646–4656.
Vogel, C.F.A., Van Winkle, L.S., Esser, C., Haarmann-Stemmann, T., 2020. The aryl hydrocarbon receptor as a target of environmental stressors - Implications for pollution mediated stress and inflammatory responses. Redox Biol. 34:101530-101530.
Wang, J., Huang, J., Wang, L., Chen, C., Yang, D., Jin, M., Bai, C., Song, Y., 2017. Urban particulate matter triggers lung inflammation via the ROS-MAPK-NF-κB signaling pathway. J Thorac Dis 9, 4398–4412.
Wang, S., Ye, J., Soong, R., Wu, B., Yu, L., Simpson, A.J., Chan, A.W.H., 2018. Relationship between chemical composition and oxidative potential of secondary organic aerosol from polycyclic aromatic hydrocarbons. Atmos. Chem. Phys. 18, 3987–4003.
World Health, O. WHO global air quality guidelines: particulate matter (PM2.5 and PM10), ozone, nitrogen dioxide, sulfur dioxide and carbon monoxide edˆeds. Geneva: World Health Organization; 2021.
Wragg, F.P.H., Fuller, S.J., Freshwater, R., Green, D.C., Kelly, F.J., Kalberer, M., 2016. An automated online instrument to quantify aerosol-bound reactive oxygen species (ROS) for ambient measurement and health-relevant aerosol studies. Atmos. Meas. Tech. 9, 4891–4900.
Wu, X., Lintelmann, J., Klingbeil, S., Li, J., Wang, H., Kuhn, E., Ritter, S., Zimmermann, R., 2017. Determination of air pollution-related biomarkers of exposure in urine of travellers between Germany and China using liquid chromatographic and liquid chromatographic-mass spectrometric methods: a pilot study. Biomarkers 22, 525–536.
Xing, Q., Wu, M., Chen, R., Liang, G., Duan, H., Li, S., Wang, Y., Wang, L., An, C., Qin, G., Sang, N., 2021. Comparative studies on regional variations in PM2.5 in the induction of myocardial hypertrophy in mice. Sci. Total Environ. 75:145179.
Ylisirniö, A., Buchholz, A., Mohr, C., Li, Z., Barreira, L., Lambe, A., Faiola, C., Kari, E., Yli-Juuti, T., Nizkorodov, S.A., Worsnop, D.R., Virtanen, A., Schobesberger, S., 2020. Composition and volatility of secondary organic aerosol (SOA) formed from oxidation of real tree emissions compared to simplified volatile organic compound (VOC) systems. Atmos. Chem. Phys. 20, 5629–5644.
Zhang, X.M., Wang, T., Hu, P., Li, B., Liu, H., Cheng, Y.F., 2019. SERPINB2 overexpression inhibited cell proliferation, invasion and migration, led to G2/M arrest, and increased radiosensitivity in nasopharyngeal carcinoma cells. J. Radiat. Res. 60, 318–327.
Zhang, Z.H., Hartner, E., Utinger, B., Gfeller, B., Paul, A., Sklorz, M., Czech, H., Yang, B. X., Su, X.Y., Jakobi, G., Orasche, J., Schnelle-Kreis, J., Jeong, S., Gröger, T., Pardo, M., Hohaus, T., Adam, T., Kiendler-Scharr, A., Rudich, Y., Zimmermann, R., Kalberer, M., 2022. Are reactive oxygen species (ROS) a suitable metric to predict toxicity of carbonaceous aerosol particles? Atmos. Chem. Phys. 22, 1793–1809.
Zhao, Z., Yang, X., Lee, J., Tolentino, R., Mayorga, R., Zhang, W., Zhang, H., 2020. Diverse Reactions in Highly Functionalized Organic Aerosols during Thermal Desorption. ACS Earth Space Chem. 4, 283–296.
Zheng, L., Liu, S., Zhuang, G., Xu, J., Liu, Q., Zhang, X., Deng, C., Guo, Z., Zhao, W., Liu, T., Wang, Y., Zhang, Y., Lin, J., Wang, Q., Sui, G., 2017. Signal Transductions of BEAS-2B Cells in Response to Carcinogenic PM2.5 Exposure Based on a Microfluidic System. Anal. Chem. 89, 5413–5421.